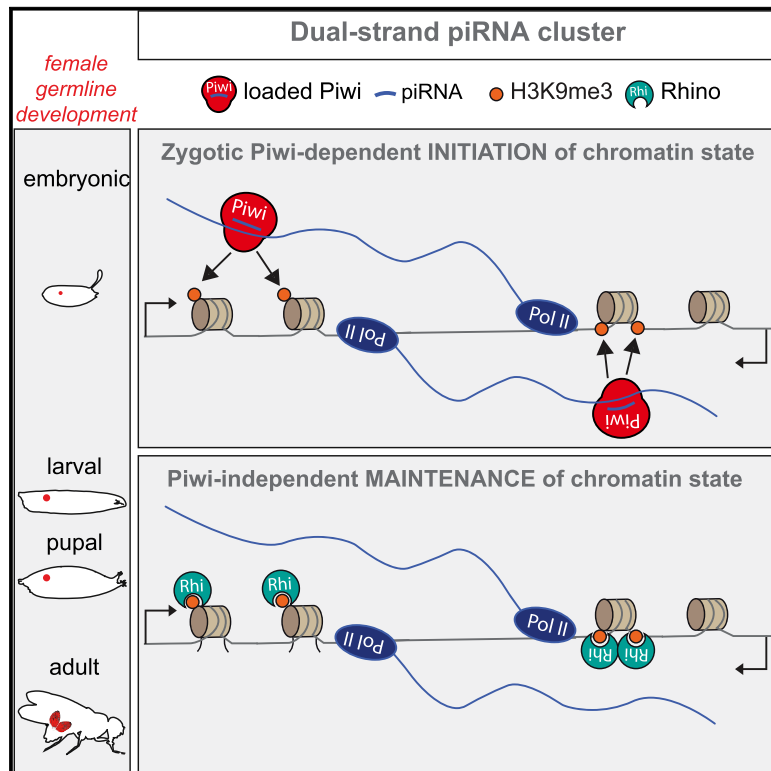


# Molecular Cell

## Piwi Is Required during *Drosophila* Embryogenesis to License Dual-Strand piRNA Clusters for Transposon Repression in Adult Ovaries

### Graphical Abstract



### Authors

Abdou Akkouche, Bruno Mugat, Bridlin Barckmann, ..., Raoul Raffel, Alain Pélisson, Séverine Chambeyron

### Correspondence

severine.chambeyron@igh.cnrs.fr

### In Brief

Piwi embryonic expression is needed for dual-strand piRNA cluster identity establishment that is required, in ovaries, for cluster H3K9 trimethylation (and Rhino binding), piRNA production, transposon repression, and female fertility. Cluster identity is then maintained in a Piwi-independent manner.

### Highlights

- Embryonic Piwi is required of piRNA production and transposon repression in adult ovaries
- Embryonic Piwi licenses piRNA clusters resulting in H3K9me3 occupancy in adults
- The embryo is the only permissive stage for piRNA cluster licensing



# Piwi Is Required during *Drosophila* Embryogenesis to License Dual-Strand piRNA Clusters for Transposon Repression in Adult Ovaries

Abdou Akkouche,<sup>1,2</sup> Bruno Mugat,<sup>1,2</sup> Bridlin Barckmann,<sup>1</sup> Carolina Varela-Chavez,<sup>1</sup> Blaise Li,<sup>1,3</sup> Raoul Raffel,<sup>1</sup> Alain Pélisson,<sup>1</sup> and Séverine Chambeyron<sup>1,4,\*</sup>

<sup>1</sup>Institut de Génétique Humaine, UMR9002 CNRS-Université de Montpellier, 34396 Montpellier, France

<sup>2</sup>These authors contributed equally

<sup>3</sup>Present address: Institut Pasteur, 25 Rue du Docteur Roux, 75015 Paris, France

<sup>4</sup>Lead Contact

\*Correspondence: [severine.chambeyron@igh.cnrs.fr](mailto:severine.chambeyron@igh.cnrs.fr)  
<http://dx.doi.org/10.1016/j.molcel.2017.03.017>

## SUMMARY

Most piRNAs in the *Drosophila* female germline are transcribed from heterochromatic regions called dual-strand piRNA clusters. Histone 3 lysine 9 trimethylation (H3K9me3) is required for licensing piRNA production by these clusters. However, it is unclear when and how they acquire this permissive heterochromatic state. Here, we show that transient Piwi depletion in *Drosophila* embryos results in H3K9me3 decrease at piRNA clusters in ovaries. This is accompanied by impaired biogenesis of ovarian piRNAs, accumulation of transposable element transcripts, and female sterility. Conversely, Piwi depletion at later developmental stages does not disturb piRNA cluster licensing. These results indicate that the identity of piRNA clusters is epigenetically acquired in a Piwi-dependent manner during embryonic development, which is reminiscent of the widespread genome reprogramming occurring during early mammalian zygotic development.

## INTRODUCTION

In animal gonads, transcriptional silencing of transposable elements (TEs) is mainly mediated by small RNAs (23–30 nt in length) called Piwi-interacting RNAs (piRNAs) because they are loaded onto Argonaute proteins (Piwi and MIWI2 in *Drosophila* and the mouse, respectively) belonging to the PIWI subfamily (Ku and Lin, 2014; Siomi et al., 2011). piRNA hybridization to nascent transcripts emanating from functional TEs inserted into euchromatin promotes the local deposition of the histone 3 lysine 9 trimethyl (H3K9me3) repressive mark in *Drosophila* or DNA methylation in the mouse (Aravin et al., 2008; Huang et al., 2013; Le Thomas et al., 2013; Sienski et al., 2012).

In the *Drosophila* ovary, most piRNAs originate from pericentromeric and subtelomeric heterochromatic regions that are highly enriched in defective TE sequences (Brennecke et al., 2007). Most of these heterochromatic regions are called dual-

strand piRNA clusters because they produce piRNAs from both genomic strands. As piRNAs originate from dual-strand clusters, they are expected to target (and, accordingly, to change the epigenetic landscape of) their own source loci. However, none of the studies performed until now has clearly reported, at a genome-wide scale, any H3K9me3 significant change, on dual-strand piRNA clusters of Piwi-depleted ovaries, comparable to the H3K9me3 heterochromatic mark reduction observed on functional euchromatic TE copies (Klenov et al., 2014; Mohn et al., 2014; Rozhkov et al., 2013).

Here, we show that initiation of the heterochromatic state at piRNA clusters requires the presence of Piwi during embryogenesis. Indeed, transient Piwi depletion in *Drosophila* embryos resulted, in ovaries, in reduced H3K9me3 occupancy at heterochromatin where piRNA clusters reside. Moreover, piRNA loss in these ovaries was associated with increased TE transcription and female sterility. Our data reveal that Piwi-associated piRNAs have an essential role during embryogenesis by driving the epigenetic licensing of piRNA source loci at pericentromeric heterochromatic regions. Once acquired in the embryo, this epigenetic landscape is maintained throughout *Drosophila* development in a Piwi-independent manner.

## RESULTS

### Piwi Depletion from the Embryo Germline Results in the Loss of H3K9me3 and Rhi on Dual-Strand piRNA Clusters in Ovaries

To transiently knock down *piwi* expression in the embryo germline (*piwi-embKD*) (Figure 1A), we expressed, throughout the entire germline development, the thermosensitive GAL80<sup>ts</sup> GAL4 inhibitor (McGuire et al., 2003) that was inactivated by a 18°C-to-28°C shift during embryogenesis to allow the *da-Gal4*-driven expression (Wodarz et al., 1995) of a *piwi* short hairpin (sh) RNAs. As a negative control (*piwi-noKD*), we bred females constantly at 18°C to prevent *piwi* knockdown (KD) (Figure 1A). We also generated a transient embryonic KD of the irrelevant *white* control gene by replacing the *shpiwi* by the *shwhite* transgene (*white-embKD*) (Figure 1A).

KD of *piwi* expression resulted in a 5- to 7-fold reduction of *piwi* RNA in 16 hr old embryos, as determined by RT-qPCR

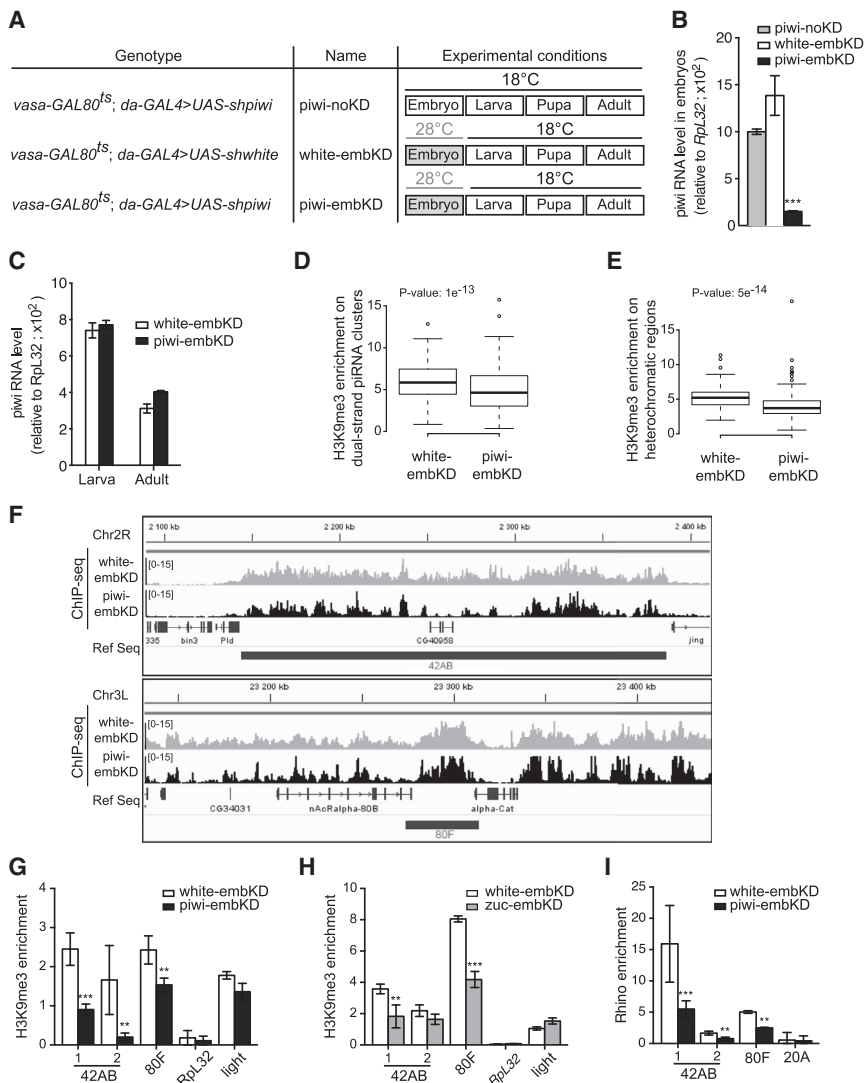


### Figure 1. KD of *piwi* in Embryos Results in H3K9me3 and Rho Depletion at Dual-Strand piRNA Clusters in Ovaries

(A) Schematic illustration of the strategy used for RNAi-mediated transient *piwi* KD in *Drosophila* embryos. Females of the *vasa-GAL80<sup>fs</sup>; da-GAL4* genotype were crossed with *UAS-shpiwi* or *UAS-shwhite* males. The progeny were raised either at 28°C (piwi-embKD and white-embKD) at the very beginning of their life (for a minimum of 3 hr and at most for 16 hr) and then kept at 18°C during the other developmental stages or at 18°C throughout development (piwi-noKD).

(B) Steady-state levels of *piwi* RNA in piwi-noKD, white-embKD, and piwi-embKD late embryos, 16 hr after egg laying (AEL), determined by RT-qPCR, and normalized to the expression of the *Rpl32* housekeeping gene. The data are the mean  $\pm$  SD of three biological replicates; \*\*\*p value < 0.005 (two-tailed Student's t test).

(C) Steady-state levels of *piwi* RNA in white-embKD and piwi-embKD larvae and ovaries, determined by RT-qPCR.

(D) Boxplots showing the distribution of H3K9me3 enrichment by ChIP-seq analysis (IP versus input reads per million) of dual-strand piRNA cluster sequences in the indicated ovarian samples. p value =  $1 \times 10^{-13}$  (pairwise Wilcoxon test).

(E) Same analysis as in (D) performed with the heterochromatin regions annotated in the *Drosophila* genome (release 5) after masking of the dual-strand piRNA cluster sequences. p value =  $5.1 \times 10^{-14}$  (pairwise Wilcoxon test).

(F) IGV Genome Browser screenshots illustrating the H3K9me3 enrichment (IP versus input) density profiles of clusters 42AB (upper) and 80F (lower). All of the signals are displayed as reads per million (RPM) values. White-embKD datasets are in gray and piwi-embKD are in black.

(G) Quantification by ChIP-qPCR of H3K9me3 enrichment at three dual-strand piRNA cluster amplicons (42AB1, 42AB2, and 80F) in white-embKD and piwi-embKD ovaries. *Rpl32* and *light* are control loci. H3K9me3 enrichment was quantified relative to the heterochromatic ribosomal

RNA gene *18S* (positive control) and normalized to input (mean  $\pm$  SD of three biological replicates); \*\*\*p value < 0.005, \*\*p value < 0.05 (two-tailed Student's t test).

(H) Same experiment as in (G), but using white-embKD and zuc-embKD ovaries.

(I) Quantification by ChIP-qPCR of Rho enrichment at three dual-strand piRNA cluster amplicons (42AB1, 42AB2, and 80F) in white-embKD and piwi-embKD ovaries. The 20A uni-strand piRNA cluster was used as negative control. The histograms show the mean  $\pm$  SD of three biological replicates; \*\*\*p value < 0.005, \*\*p value < 0.05 (two-tailed Student's t test). See also Figure S1.

(Figure 1B). Moreover, our *piwi* KD approach seemed more efficient than the previously published conditions (Rozhkov et al., 2013; Mohn et al., 2014), as judged by immunofluorescence microscopy of whole-mount late-stage embryos (Figure S1A). Finally, compared with control white-embKD embryos, the level of two germline-dominant TEs (HeT-A and HMS-Beagle), which are mainly expressed in the germline, but not of the soma-dominant TE Tabor, was upregulated in piwi-embKD (Figure S1B), thus functionally validating the germline *piwi* KD. In agreement with a recent observation (Marie et al., 2016), this finding also indicates that zygotic Piwi expression in the germline is required for TE repression during *Drosophila* embryonic development. To confirm that the effect of *piwi* KD was restricted to the embry-

onic stage of development, we quantified *piwi* mRNA levels at other stages (kept at 18°C). The amount of *piwi* RNA was very similar in piwi-embKD and white-embKD larvae and adult ovaries (Figure 1C), confirming that *piwi* expression returned to normal levels after the transient embryonic KD.

To determine whether transient Piwi depletion from the embryo germline affected the heterochromatin epigenetic landscape, we compared the accumulation of H3K9me3 in piwi-embKD and white-embKD ovaries. We immunoprecipitated chromatin from ovaries with an anti-H3K9me3 antibody and then deep sequenced both the input and immunoprecipitated chromatin (ChIP-seq). Analysis of H3K9me3 enrichment using pooled ChIP-seq unique mapper reads from independent

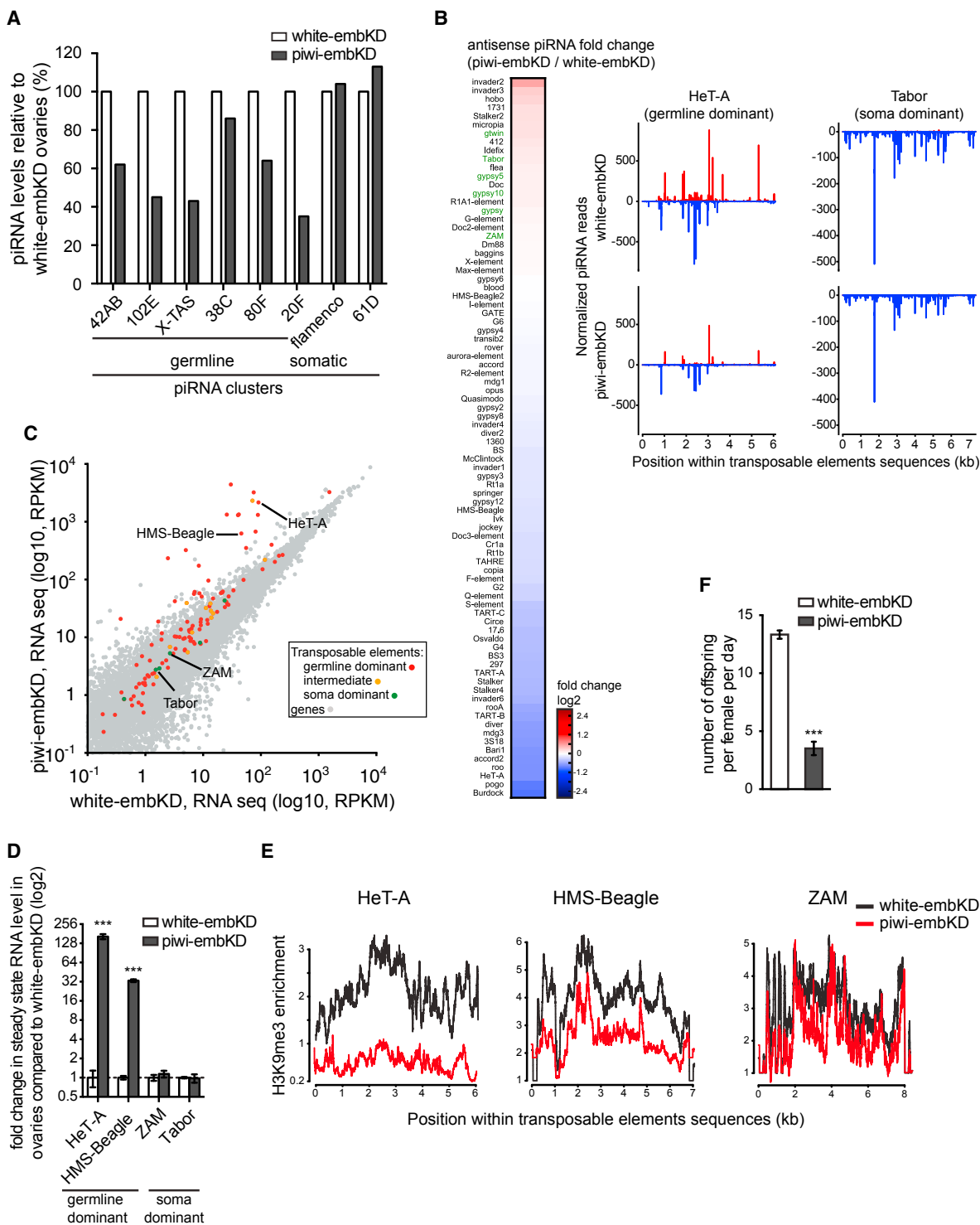


**Figure 2. KD of *piwi* in the Embryo Results in piRNA Loss, Transposable Element Overexpression, and Sterility in Adult Females**

(A) Histogram showing the loss of ovarian piRNAs originating from germinal dual-strand piRNA clusters after Piwi embryonic depletion (piwi-embKD) compared with control (white-embKD). The piRNAs produced by the somatic flamenco and 61D clusters were not lost in piwi-embKD ovaries. Only the reads uniquely mapped to piRNA clusters were used and normalized to miRNA reads.

(B) Left: Heatmap representing the fold change of antisense TE piRNA accumulation (normalized to miRNA reads) in piwi-embKD versus white-embKD ovaries. The most highly targeted TE families (i.e., those for which at least 1,500 reads were sequenced) were studied. Soma-dominant TEs are written in green. The

(legend continued on next page)

biological replicates showed that compared with control ovaries, H3K9me3 was depleted at dual-strand piRNA clusters (Figures 1D and 1F) and also at non-piRNA cluster heterochromatic regions in piwi-embKD ovaries (Figure 1E). We confirmed H3K9me3 depletion on dual-strand clusters by ChIP-qPCR analysis of three amplicons, two located in the 42AB and one in the 80F germline dual-strand piRNA clusters (Figure 1G).

To further confirm the importance of the piRNA pathway in H3K9me3 accumulation at piRNA clusters, we performed transient embryonic KD of *zuc* (*zuc*-embKD). The *zuc* gene encodes the endonuclease Zucchini that is required for the biogenesis of Piwi-bound piRNAs (Han et al., 2015; Mohn et al., 2015). Its KD resulted in a slight decrease of Piwi accumulation in late embryos (Figure S1C). ChIP-qPCR analysis of *zuc*-embKD ovaries revealed that, like in piwi-embKD ovaries, H3K9me3 at the 42AB and 80F germline dual-strand piRNA clusters was significantly decreased compared with white-embKD ovaries (Figure 1H). These data provide evidence for a positive effect of embryonic piwi expression on H3K9me3 occupancy at dual-strand piRNA clusters in the ovary.

The *Drosophila* HP1 homolog Rhi binds directly to H3K9me3 at dual-strand piRNA clusters (Klattenhoff et al., 2009; Le Thomas et al., 2014a; Mohn et al., 2014). Consistently, ChIP-qPCR analysis showed that Rhi binding to dual-strand piRNA clusters was significantly lower in piwi-embKD than in control white-embKD ovaries (Figure 1I). We conclude that during *Drosophila* embryogenesis, Piwi and the piRNA pathway are required for the typical accumulation of H3K9me3 and Rhi in ovaries that defines the identity of dual-strand piRNA clusters.

### Piwi Embryonic Expression Is Critical for piRNA-Mediated Repression of TEs in the Adult Germline

Previous studies have shown that the presence of Rhi on dual-strand piRNA clusters directly correlates with the production of piRNAs (Klattenhoff et al., 2009; Mohn et al., 2014; Zhang et al., 2014). To test whether the reduction of Rhi binding observed in piwi-embKD ovaries affected the production of piRNAs in the adult, we made libraries of small (18–30 nt) RNAs from piwi-embKD, white-embKD, and piwi-noKD ovaries, and then sequenced and analyzed their small RNA populations (Table S1). The libraries were normalized to the number of microRNA reads (Figure 2) or of unique mapper reads of flamenco, a soma-specific single-strand piRNA cluster (Figure S2). Comparison of the number of piRNAs that mapped uniquely to dual-strand piRNA clusters indicated that the level of piRNAs derived from germline dual-strand clusters was markedly reduced in

piwi-embKD compared with white-embKD ovaries (Figures 2A and S2A). Conversely, piRNAs derived from soma-specific clusters were unchanged. These observations show that Piwi expression in the embryo is required for optimal piRNA production from dual-strand piRNA clusters in the adult female germline. Moreover, the antisense piRNAs that target germline-dominant TEs were significantly reduced in piwi-embKD ovaries compared with control ovaries (Figures 2B and S2B). Conversely, accumulation of soma-dominant TE antisense piRNAs was not affected (green TEs in Figures 2B and S2B). We confirmed this finding by analyzing a second independent piwi-embKD library and by comparing the data with those of another white-embKD library (Figure S2C; Table S1) and with the piwi-noKD control library (Figure S2D; Table S1). We also checked that the variability of antisense piRNAs between controls was low (Figure S2E).

The decrease in antisense piRNAs should threaten genome integrity due to TE overexpression. We thus compared the steady-state levels of RNAs transcribed from TEs in piwi-embKD and white-embKD ovaries by transcriptome profiling. We observed no effect on gene expression and an increase of some TE transcripts in piwi-embKD ovaries compared with white-embKD ovaries (Figures 2C and S2F). Interestingly, derepression occurred mostly at TEs where piRNA levels were lower in piwi-embKD ovaries compared with white-embKD ovaries (Figure S2G). We confirmed these RNA-seq data by RT-qPCR analysis of two upregulated TEs in piwi-embKD ovaries (Figure 2D). Furthermore, in situ hybridization of whole-mount ovaries with HeT-A and HMS-Beagle fluorescent riboprobes showed that these TE transcripts accumulated in the oocytes of piwi-embKD adults (Figure S2H).

To assess whether the increased expression of TEs in piwi-embKD ovaries was accompanied by loss of H3K9me3 from these loci, we analyzed the ChIP-seq libraries presented above. Compared with control white-embKD ovaries, in piwi-embKD ovaries, H3K9me3 was depleted at chromatin of germline-dominant TEs, but not of soma-dominant TEs (Figure 2E). We confirmed H3K9me3 depletion at HeT-A in piwi-embKD ovaries also by ChIP-qPCR (Figure S2I). Altogether, these data suggest that the TE overexpression observed in the adult female germline after transient piwi KD during embryogenesis occurs at the transcriptional level, probably as a result of H3K9me3 depletion from the TE chromatin.

TE expression in the germline has been correlated with loss of fertility (Siomi et al., 2011). To investigate whether activation of TE expression after transient Piwi KD could result in an adult

density profiles, normalized to miRNAs, of piRNA reads that mapped to HeT-A, a germline-dominant TE, and to Tabor, a soma-dominant TE (sense reads: up in red and antisense reads: down in blue) are shown (right).

(C) Scatterplot comparing the number of RNA-seq reads (per kilobase per million genome-matching reads [RPKM]) that matched annotated genes or TEs in white-embKD or piwi-embKD ovaries (log<sub>10</sub> scale).

(D) Bar plot showing the fold change in steady-state RNA level of two germline-dominant and two soma-dominant TEs in piwi-embKD and white-embKD ovaries. The RT-PCR quantification was done relative to *RpL32* expression.

(E) Effect of Piwi embryonic depletion on TE chromatin state in the ovary. The normalized density profiles of the H3K9me3 repressive mark on germline-dominant (HeT-A and HMS-Beagle) and soma-dominant (ZAM) TE consensus sequences are shown. The red and black lines represent H3K9me3 enrichment relative to input in piwi-embKD and white-embKD ovaries, respectively.

(F) Number of offspring produced per female per day after transient KD of *piwi* (piwi-embKD) or *white* (white-embKD) during embryogenesis. The histograms in (D) and (F) represent the mean ± SD of three and four biological replicates, respectively; \*\*\*p value < 0.005 (two-tailed Student's t test). See also Figure S2.

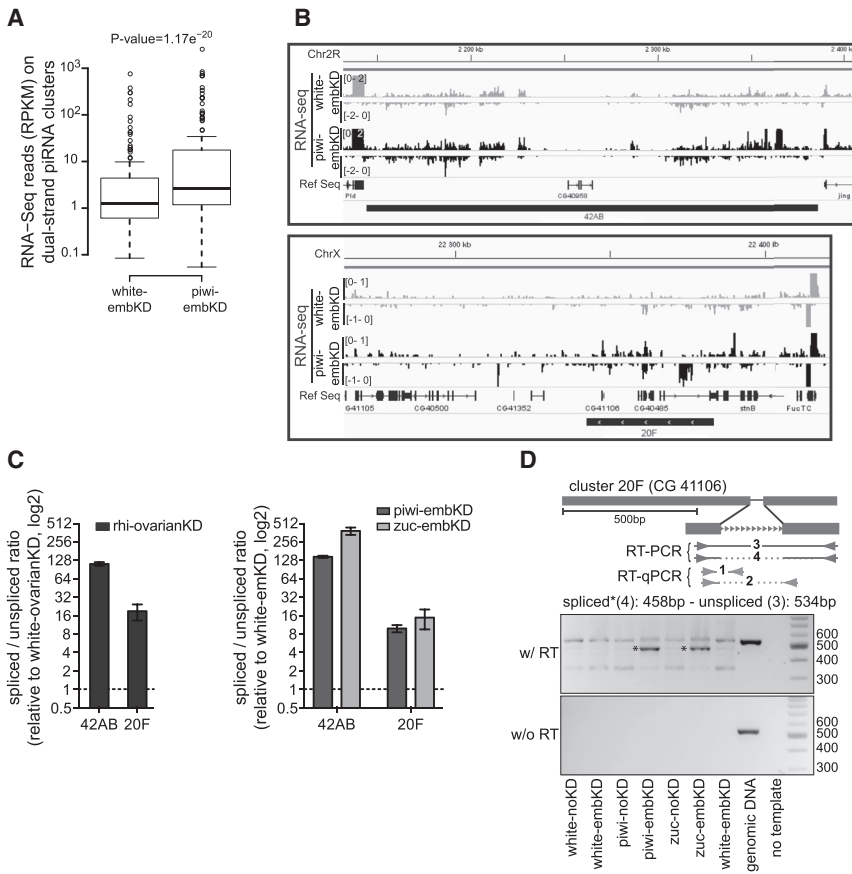


### Figure 3. Piwi Embryonic Expression Is Required for the Licensing of Dual-Strand piRNA Clusters to Produce Unspliced piRNA Precursors in Ovaries

(A) Boxplots showing the distribution of normalized RNA-seq signals (reads per kilobase per million mapped reads [RPKM]), obtained using the piPipes tool to standardize RNA-seq data analysis (Han et al., 2014), at bins belonging to dual-strand piRNA clusters in white-embKD and piwi-embKD ovarian samples.  $p$  value =  $1.17 \times 10^{-20}$  (pairwise Wilcoxon test).

(B) IGV Genome Browser screenshots of cluster 42AB (upper) and cluster 20F (lower) RNA-seq signals displayed as reads per million (RPM) values and mapped to the Watson (+) and Crick (-) orientation. White-embKD datasets are in gray and piwi-embKD are in black.

(C) Strand-specific RT-qPCR was used to study the splicing of transcripts isolated from rhi-ovarianKD (left) and from piwi-embKD and zuc-embKD ovaries (right) at two splicing sites located in dual-strand piRNA clusters. The first one, previously described, is in the 42AB cluster, and the second one corresponds to the intron of the *CG41106* gene in the 20F cluster (see the gray amplicons in Figure 3D; 1: unspliced and 2: spliced). The spliced and unspliced amplicons were quantified relative to *RpL32* expression and the spliced/unspliced ratio was normalized to the ratio of the white-embKD control experiment for embryonic knockdown and of the white-ovarianKD control experiment for ovarian knockdown. The data are the mean  $\pm$  SD of three biological replicates.

(D) Detection by semiquantitative RT-PCR of splicing of the *CG41106* intron located in cluster 20F (black amplicons: the spliced amplicon 4 is indicated by a star on the gel). The reverse transcription reaction was performed with (w/RT) and without (w/oRT) reverse transcriptase. See also Figure S3.

phenotype, we counted the number of offspring produced per female and per day and found a clear fertility defect in piwi-embKD females compared with white-embKD controls (Figure 2F). This dramatic effect on fertility highlights the important functional significance for female gametogenesis of Piwi expression very early in development.

### Piwi Embryonic Expression Is Required for the Licensing of Dual-Strand piRNA Clusters to Produce Unspliced piRNA Precursors in Ovaries

Rhi binding to H3K9me3 is required for efficient ovarian transcription of dual-strand piRNA clusters (Mohn et al., 2014). However, embryonic piwi KD resulted in H3K9me3 depletion on dual-strand piRNA cluster in ovaries, but did not cause a decrease of their transcripts (Figures 3A, 3B, and S3A). Therefore, the association of piRNA depletion with a slight accumulation of piRNA cluster transcripts in Piwi-embKD ovaries suggests that these transcripts are not processed into piRNAs as efficiently as in control ovaries.

We took advantage of this unusual production of transcripts by Rhi-depleted piRNA clusters to investigate the repressive role of Rhi on splicing (Chen et al., 2016; Zhang et al., 2014). We studied by strand-specific RT-qPCR the splicing at four spliced sites: one in the 42AB dual-strand piRNA cluster (previously described

by Zhang et al., 2014) and three in the protein-coding genes *CG8671*, *garnet*, and *CG41106* (this last one is embedded in the 20F dual-strand piRNA cluster). As a positive control, we knocked down *rhi* expression in adult ovaries by shifting the temperature to 28°C after the emergence of adults (rhi-ovarianKD). As expected, *rhi* mRNA depletion (Figure S3B) correlated with a dramatic increase of the spliced-to-unspliced ratios of both cluster-related amplicons (Figure 3C, left). A strikingly similar increase occurred also in both piwi-embKD and zuc-embKD ovaries compared with white-embKD control ovaries (Figure 3C, right). Conversely, splicing of the two non-cluster-associated protein-coding RNAs was unaffected (Figure S3C). This spliced/unspliced ratio change was mainly the result of increased spliced RNA levels (Figure S3D). This effect was not due to a difference in genetic background between the piRNA pathway KD samples and the white-embKD control, as indicated by the absence of spliced transcripts in the piwi-noKD and zuc-noKD isogenic controls (Figure 3D).

We then used the piwi-embKD and white-embKD adult ovarian transcriptomic data to determine genome-wide whether this effect on dual-strand piRNA cluster splicing was specific and general. We first checked that the splicing of protein-coding genes was unchanged between piwi-embKD and white-embKD ovaries (Figure S3E). Then, using the splicing of genes as a

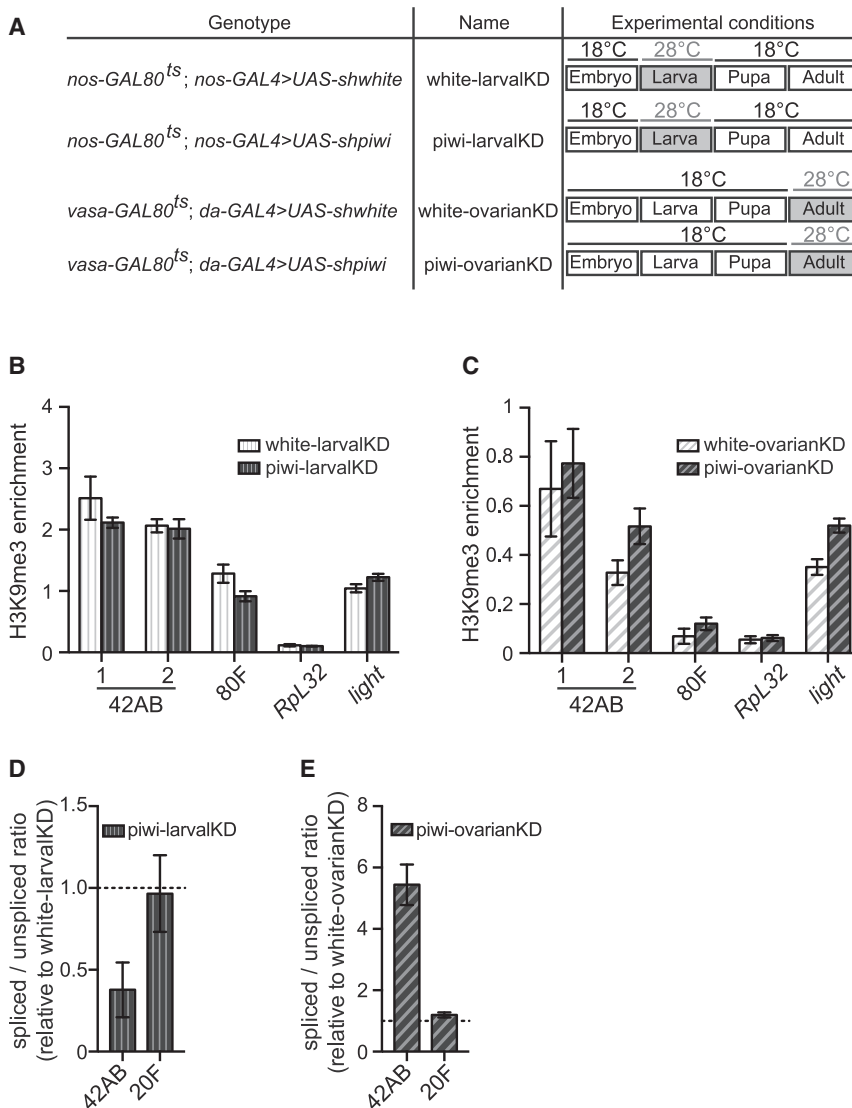


**Figure 4. The Embryo Is the Only Piwi-Sensitive Developmental Stage for Piwi-Mediated Dual-Strand piRNA Cluster Licensing**

(A) Schematic illustration of the strategy used for RNAi-mediated transient piwi KD in larvae and adults.

(B) ChIP-qPCR quantification of H3K9me3 enrichment at three dual-strand piRNA cluster amplicons in ovaries after KD of *white* (white-larvalKD) or *piwi* (piwi-larvalKD) at the larval stage. *RplL32* and *light* were used as controls. H3K9me3 enrichment was quantified relative to the ribosomal RNA gene *18S* (positive control) and normalized to input. The histograms show the mean  $\pm$  SD of three biological replicates.

(C) Same experiment as in (B), but after KD of *white* (white-ovarianKD) or *piwi* (piwi-ovarianKD) at the adult stage.

(D and E) Splicing assayed by strand-specific RT-qPCR at dual-strand piRNA cluster spliced sites (see Figure 3C for details) in the adult ovaries after KD of *piwi* at the larval stage (piwi-larvalKD) (D) or at the adult stage (piwi-ovarianKD) (E). See also Figure S4.

We also knocked down *piwi* in adult ovaries by shifting the temperature to 28°C after the emergence of adults (piwi-ovarianKD) (Figure 4A). We confirmed the loss of Piwi protein by whole-mount immunofluorescence analysis of ovaries (Figure S4C) and the reduction of *piwi* RNA by RT-qPCR (Figure S4D). Although Piwi depletion from adult ovaries correlated with germline-dominant TE mRNA accumulation (Figure S4D), it did not have any significant effect on H3K9me3 enrichment (Figure 4C) or on the splicing of the gene inserted in the 20F cluster (Figure 4E). We observed a small increase of 42AB splicing (Figure 4E), but this could

be explained by derepression of another gypsy12 copy elsewhere in the genome.

normalizer, we demonstrated that transient Piwi depletion from embryos had a genome-wide and significant positive effect on the splicing efficiency only of dual strand piRNA clusters (Figures S3F and S3G).

### Embryogenesis Is the Only Developmental Stage for Piwi-Mediated Dual-Strand piRNA Cluster Licensing

To determine whether dual-strand piRNA cluster licensing requires Piwi expression also later in development, we induced shRNA expression during the larval stage (piwi-larvalKD) (Figure 4A). Piwi expression in the germline was almost completely abolished at the larval stage, as indicated by whole-mount immunofluorescence analysis of L3 female gonads using an anti-Piwi antibody (Figure S4A). Piwi depletion at the larval stage did not affect H3K9me3 accumulation at the 42AB and 80F regions (ChIP-qPCR of ovaries) (Figure 4B), splicing of the 42AB and 20F amplicons (RT-qPCR of ovaries) (Figure 4D), or female fertility (Figure S4B).

By reviewing published genome-wide ChIP-seq data on adult ovaries (Mohn et al., 2014), we found that Piwi germinal depletion (piwi-GLKD) did not decrease H3K9me3 occupancy at constitutive heterochromatin, including dual-strand piRNA cluster sequences (Figures S4E and S4F).

Therefore, as far as we have tested, the embryo is the only developmental stage when Piwi depletion can influence H3K9me3 deposition at and piRNA production by, dual-strand piRNA clusters in the ovary.

## DISCUSSION

In this study, we show that transient embryonic Piwi depletion causes the reduction of H3K9me3 occupancy at piRNA-source-containing heterochromatic regions in the adult female germline. This results in reduced Rhi binding to dual-strand

piRNA cluster chromatin (Figure 1). These chromatin changes affect dual-strand piRNA cluster transcription and piRNA precursor maturation (Figure 3), leading to germline piRNA loss and to TE derepression in ovaries (Figure 2). Conversely, Piwi depletion at the larval and adult stages does not have such effects (Figure 4). These observations indicate that the ability of dual-strand piRNA clusters to produce piRNAs in the ovary is specifically determined by Piwi expression in the embryo, and not at other developmental stages.

### Role of Maternal and Zygotic piRNAs in piRNA Cluster Licensing

In *Drosophila* early embryos, both piRNAs and PIWI proteins are inherited from the maternal germline (Brennecke et al., 2008; Grentzinger et al., 2012). Moreover, piRNA cluster activity in the adult female germline requires the previous deposition of these maternal piRNAs in the embryo (Le Thomas et al., 2014a; Le Thomas et al., 2014b; de Vanssay et al., 2012). Similarly to the Piwi zygotic effect reported here, this maternal effect is also associated with H3K9me3 deposition on and Rhi binding to ovarian dual-strand piRNA clusters (Le Thomas et al., 2014a). Therefore, both maternal and zygotic piRNAs appear to be necessary to fully establish the chromatin landscape that specifies dual-strand piRNA cluster identity in the adult female germline. Similar maternal and zygotic Piwi requirements were reported for the establishment of constitutive heterochromatin in *Drosophila* somatic tissues (Gu and Elgin, 2013).

The model presented in Figure S4G speculates about how and when piRNA cluster licensing is established during embryogenesis. It proposes that piRNA clusters can be transcribed before zygotic genome activation. Nascent transcripts emanating from these TE-rich regions during this very early transcription phase are targeted by Piwi-associated maternal piRNAs to allow the subsequent recruitment of histone-modifying complexes, leading to H3K9me3 deposition on cognate sequences. The resulting chromatin changes license piRNA cluster transcription for de novo production of zygotic piRNAs that are required for full piRNA cluster licensing. Further testing of this working model will need the detailed characterization of the embryonic and ovarian phenotypes after embryonic piRNA pathway depletion at specific temporal windows.

These two putative steps in our model, in which the maternal piRNA population initiates a specific chromatin environment in the embryo to allow the production of new piRNAs that are themselves required for the production of ovarian piRNAs at much later stages, are reminiscent of the non-coding RNA-based targeting strategy used by *S. pombe* for pericentromeric heterochromatin assembly (Holoach and Moazed, 2015).

### Piwi-Dependent versus Piwi-Independent Maintenance of Chromatin Landscapes

Several studies have demonstrated that Piwi has an essential role in the deposition of H3K9 methylation (a repressive chromatin mark) on euchromatic TE copies, resulting in TE transcriptional silencing in the *Drosophila* ovary. This heterochromatinization also allows TEs to become germline piRNA producers, called piRNA source loci (Mohn et al., 2014; Shpiz et al., 2014). Like Piwi-mediated dual-strand piRNA cluster licensing (this

study), acquisition of this new epigenetic feature by TEs can be at least partly explained by Rhi binding to H3K9me3. However, differently from piRNA clusters, this epigenetic state must be continuously maintained on TEs in a Piwi-dependent manner. In fact, Piwi ovarian depletion simultaneously reduces TE transcriptional silencing, H3K9 methylation at TEs, and piRNA production by these TE sequences (Mohn et al., 2014). This is reminiscent of the establishment and maintenance of the *HM* silent chromatin state in budding yeast by silencers that mediate the establishment of hypoacetylated domains and that are continuously required for the maintenance of this silent state (Cheng and Gartenberg, 2000).

Conversely, the H3K9me3 mark present on dual-strand piRNA clusters is not affected by Piwi ovarian depletion (Figure 4C). These data suggest that H3K9me3 enrichment at dual-strand piRNA clusters is maintained through another mechanism that does not require Piwi expression in larval and adult ovaries. The same developmental dynamics was described in *Drosophila* somatic tissues where embryonic Piwi is required for the assembly of a heterochromatic state that is subsequently maintained, throughout development, in the absence of Piwi expression (Gu and Elgin, 2013).

### STAR★METHODS

Detailed methods are provided in the online version of this paper and include the following:

- KEY RESOURCES TABLE
- CONTACT FOR REAGENT AND RESSOURCES SHARING
- METHOD DETAILS
  - *Drosophila* stocks
  - Construction of transgenic fly stocks
  - Stage-specific depletion of the protein of interest during *Drosophila* development
  - Fertility test
  - RNA extraction and RT-qPCR
  - Small RNA purification and sequencing
  - ChIP-seq and ChIP-qPCR
  - RNA-seq
  - RNA fluorescent in situ hybridization and immunofluorescence
  - Western blot analysis
  - Computational Analysis
- QUANTIFICATION AND STATISTICAL ANALYSIS
- DATA AND SOFTWARE AVAILABILITY

### SUPPLEMENTAL INFORMATION

Supplemental Information includes four figures and two tables and can be found with this article online at <http://dx.doi.org/10.1016/j.molcel.2017.03.017>.

### AUTHOR CONTRIBUTIONS

A.A. and B.M. performed most of the experiments and C.V.-C. performed the FISH experiments. B.M. prepared the figures; B.L. performed small RNA-seq; R.R. performed the ChIP-seq; and B.B. performed the RNA-seq analysis and western blot. A.A., A.P., and S.C. designed the experiments, analyzed the data, and wrote the paper.

## ACKNOWLEDGMENTS

We thank Hervé Seitz for assistance and discussions; J. Brennecke and K. Mochizuki for their comments on the manuscript; Elisabetta Andermarcher for manuscript editing; M. Siomi, J. Brennecke, W.E. Theurkauf, and D. Godt for providing antibodies; and R.L. Davis, J. Bischof, and Elena Casacuberta for providing vectors. Stocks obtained from the Bloomington Drosophila Stock Center (NIH P40OD018537) were used in this study. This work was supported by The Centre National de la Recherche Scientifique (CNRS), the Fondation pour la Recherche Médicale (FRM), grant number (DEP20131128518, to S.C.), the Fondation ARC pour la Recherche sur le Cancer, and the ANR (ESSOR-JCJC-1604041). We thank the Montpellier RIO Imaging facility for help with image acquisition and analysis. A.A. was supported by the "Fondation ARC- Aides post-doctorales", C.V.-C. by FRM, B.L. by the ANR, and B.B. by CNRS.

Received: September 16, 2016

Revised: January 13, 2017

Accepted: March 24, 2017

Published: April 27, 2017

## REFERENCES

- Aravin, A.A., Sachidanandam, R., Bourc'his, D., Schaefer, C., Pezic, D., Toth, K.F., Bestor, T., and Hannon, G.J. (2008). A piRNA pathway primed by individual transposons is linked to de novo DNA methylation in mice. *Mol. Cell* **31**, 785–799.
- Bischof, J., Maeda, R.K., Hediger, M., Karch, F., and Basler, K. (2007). An optimized transgenesis system for Drosophila using germ-line-specific phiC31 integrases. *Proc. Natl. Acad. Sci. USA* **104**, 3312–3317.
- Brennecke, J., Aravin, A.A., Stark, A., Dus, M., Kellis, M., Sachidanandam, R., and Hannon, G.J. (2007). Discrete small RNA-generating loci as master regulators of transposon activity in Drosophila. *Cell* **128**, 1089–1103.
- Brennecke, J., Malone, C.D., Aravin, A.A., Sachidanandam, R., Stark, A., and Hannon, G.J. (2008). An epigenetic role for maternally inherited piRNAs in transposon silencing. *Science* **322**, 1387–1392.
- Chen, Y.-C.A., Stuwe, E., Luo, Y., Ninova, M., Le Thomas, A., Rozhavskaia, E., Li, S., Vempati, S., Laver, J.D., Patel, D.J., et al. (2016). Cutoff suppresses RNA polymerase II termination to ensure expression of piRNA precursors. *Mol. Cell* **63**, 97–109.
- Cheng, T.H., and Gartenberg, M.R. (2000). Yeast heterochromatin is a dynamic structure that requires silencers continuously. *Genes Dev.* **14**, 452–463.
- de Vanssay, A., Bougé, A.-L., Boivin, A., Hermant, C., Teyssset, L., Delmarre, V., Antoniewski, C., and Ronsseray, S. (2012). Paramutation in Drosophila linked to emergence of a piRNA-producing locus. *Nature* **490**, 112–115.
- Dobin, A., Davis, C.A., Schlesinger, F., Drenkow, J., Zaleski, C., Jha, S., Batut, P., Chaisson, M., and Gingeras, T.R. (2013). STAR: ultrafast universal RNA-seq aligner. *Bioinformatics* **29**, 15–21.
- Grentzinger, T., and Chambeyron, S. (2014). Fast and accurate method to purify small noncoding RNAs from Drosophila ovaries. In *PIWI-Interacting RNAs*, M.C. Siomi, ed. (Humana Press), pp. 171–182.
- Grentzinger, T., Armenise, C., Brun, C., Mugat, B., Serrano, V., Pelisson, A., and Chambeyron, S. (2012). piRNA-mediated transgenerational inheritance of an acquired trait. *Genome Res.* **22**, 1877–1888.
- Gu, T., and Elgin, S.C. (2013). Maternal depletion of Piwi, a component of the RNAi system, impacts heterochromatin formation in Drosophila. *PLoS Genet.* **9**, e1003780.
- Han, B.W., Wang, W., Zamore, P.D., and Weng, Z. (2014). piPipes: a set of pipelines for piRNA and transposon analysis via small RNA-seq, RNA-seq, degradome- and CAGE-seq, ChIP-seq and genomic DNA sequencing. *Bioinformatics* **31**, 593–595.
- Han, B.W., Wang, W., Li, C., Weng, Z., and Zamore, P.D. (2015). Noncoding RNA. piRNA-guided transposon cleavage initiates Zucchini-dependent, phased piRNA production. *Science* **348**, 817–821.
- Holoch, D., and Moazed, D. (2015). RNA-mediated epigenetic regulation of gene expression. *Nat. Rev. Genet.* **16**, 71–84.
- Huang, X.A., Yin, H., Sweeney, S., Raha, D., Snyder, M., and Lin, H. (2013). A major epigenetic programming mechanism guided by piRNAs. *Dev. Cell* **24**, 502–516.
- Jones, E., Oliphant, E., Peterson, P., et al. (2001). SciPy: open source scientific tools for python, <http://www.scipy.org/>.
- Klattenhoff, C., Xi, H., Li, C., Lee, S., Xu, J., Khurana, J.S., Zhang, F., Schultz, N., Koppetsch, B.S., Nowosielska, A., et al. (2009). The Drosophila HP1 homolog Rhino is required for transposon silencing and piRNA production by dual-strand clusters. *Cell* **138**, 1137–1149.
- Klenov, M.S., Lavrov, S.A., Korb, A.P., Stolyarenko, A.D., Yakushev, E.Y., Reuter, M., Pillai, R.S., and Gvozdev, V.A. (2014). Impact of nuclear Piwi elimination on chromatin state in Drosophila melanogaster ovaries. *Nucleic Acids Res.* **42**, 6208–6218.
- Köster, J., and Rahmann, S. (2012). Snakemake—a scalable bioinformatics workflow engine. *Bioinformatics* **28**, 2520–2522.
- Ku, H.-Y., and Lin, H. (2014). PIWI proteins and their interactors in piRNA biogenesis, germline development and gene expression. *Natl. Sci. Rev.* **1**, 205–218.
- Langmead, B., and Salzberg, S.L. (2012). Fast gapped-read alignment with Bowtie 2. *Nat. Methods* **9**, 357–359.
- Le Thomas, A., Rogers, A.K., Webster, A., Marinov, G.K., Liao, S.E., Perkins, E.M., Hur, J.K., Aravin, A.A., and Tóth, K.F. (2013). Piwi induces piRNA-guided transcriptional silencing and establishment of a repressive chromatin state. *Genes Dev.* **27**, 390–399.
- Le Thomas, A., Stuwe, E., Li, S., Du, J., Marinov, G., Rozhkov, N., Chen, Y.-C.A., Luo, Y., Sachidanandam, R., Toth, K.F., et al. (2014a). Transgenerationally inherited piRNAs trigger piRNA biogenesis by changing the chromatin of piRNA clusters and inducing precursor processing. *Genes Dev.* **28**, 1667–1680.
- Le Thomas, A., Marinov, G.K., and Aravin, A.A. (2014b). A transgenerational process defines piRNA biogenesis in Drosophila virilis. *Cell Rep.* **8**, 1617–1623.
- Li, H., and Durbin, R. (2010). Fast and accurate long-read alignment with Burrows–Wheeler transform. *Bioinformatics* **26**, 589–595.
- Livak, K.J., and Schmittgen, T.D. (2001). Analysis of relative gene expression data using real-time quantitative PCR and the 2(-Delta Delta C(T)) method. *Methods* **25**, 402–408.
- Marie, P.P., Ronsseray, S., and Boivin, A. (2016). From embryo to adult: piRNA-mediated silencing throughout germline development in Drosophila. *G3* **7**, 505–516.
- McGuire, S.E., Le, P.T., Osborn, A.J., Matsumoto, K., and Davis, R.L. (2003). Spatiotemporal rescue of memory dysfunction in Drosophila. *Science* **302**, 1765–1768.
- Mohn, F., Sienski, G., Handler, D., and Brennecke, J. (2014). The rhino-deadlock-cutoff complex licenses noncanonical transcription of dual-strand piRNA clusters in Drosophila. *Cell* **157**, 1364–1379.
- Mohn, F., Handler, D., and Brennecke, J. (2015). Noncoding RNA. piRNA-guided slicing specifies transcripts for Zucchini-dependent, phased piRNA biogenesis. *Science* **348**, 812–817.
- Mugat, B., Akkouche, A., Serrano, V., Armenise, C., Li, B., Brun, C., Fulga, T.A., Van Vactor, D., Pelisson, A., and Chambeyron, S. (2015). MicroRNA-dependent transcriptional silencing of transposable elements in Drosophila follicle cells. *PLoS Genet.* **11**, e1005194.
- Ramírez, F., Ryan, D.P., Grüning, B., Bhardwaj, V., Kilpert, F., Richter, A.S., Heyne, S., Dündar, F., and Manke, T. (2016). deepTools2: a next generation web server for deep-sequencing data analysis. *Nucleic Acids Res.* **44**, W160–W165.
- Roberts, A., and Pachter, L. (2011). RNA-Seq and find: entering the RNA deep field. *Genome Med.* **3**, 74.
- Roberts, A., Trapnell, C., Donaghey, J., Rinn, J.L., and Pachter, L. (2011). Improving RNA-Seq expression estimates by correcting for fragment bias. *Genome Biol.* **12**, R22.

- Rozhkov, N.V., Hammell, M., and Hannon, G.J. (2013). Multiple roles for Piwi in silencing *Drosophila* transposons. *Genes Dev.* *27*, 400–412.
- Shpiz, S., Ryazansky, S., Olovnikov, I., Abramov, Y., and Kalmykova, A. (2014). Euchromatic transposon insertions trigger production of novel Pi- and endo-siRNAs at the target sites in the *Drosophila* germline. *PLoS Genet.* *10*, e1004138.
- Sienski, G., Dönertas, D., and Brennecke, J. (2012). Transcriptional silencing of transposons by Piwi and maelstrom and its impact on chromatin state and gene expression. *Cell* *151*, 964–980.
- Siomi, M.C., Sato, K., Pezic, D., and Aravin, A.A. (2011). PIWI-interacting small RNAs: the vanguard of genome defence. *Nat. Rev. Mol. Cell Biol.* *12*, 246–258.
- Trapnell, C., Pachter, L., and Salzberg, S.L. (2009). TopHat: discovering splice junctions with RNA-Seq. *Bioinformatics* *25*, 1105–1111.
- Trapnell, C., Williams, B.A., Pertea, G., Mortazavi, A., Kwan, G., van Baren, M.J., Salzberg, S.L., Wold, B.J., and Pachter, L. (2010). Transcript assembly and abundance estimation from RNA-Seq reveals thousands of new transcripts and switching among isoforms. *Nat. Biotechnol.* *28*, 511–515.
- Wodarz, A., Hinz, U., Engelbert, M., and Knust, E. (1995). Expression of crumbs confers apical character on plasma membrane domains of ectodermal epithelia of *Drosophila*. *Cell* *82*, 67–76.
- Zhang, Z., Theurkauf, W.E., Weng, Z., and Zamore, P.D. (2012). Strand-specific libraries for high throughput RNA sequencing (RNA-Seq) prepared without poly(A) selection. *Silence* *3*, 9.
- Zhang, Z., Wang, J., Schultz, N., Zhang, F., Parhad, S.S., Tu, S., Vreven, T., Zamore, P.D., Weng, Z., and Theurkauf, W.E. (2014). The HP1 homolog rhino anchors a nuclear complex that suppresses piRNA precursor splicing. *Cell* *157*, 1353–1363.

## STAR★METHODS

## KEY RESOURCES TABLE

REAGENT or RESOURCE	SOURCE	IDENTIFIER
<b>Antibodies</b>		
Rabbit polyclonal anti-Piwi (d-190)	Santa Cruz Biotechnology	cat# sc98264
Rat monoclonal anti-Vasa	DSHB	cat# AB_760351
Guinea pig anti Rhino	W. Theurkauf	N/A
Anti-Histone H3 (tri methyl K9) antibody -ChIP grade	Abcam	cat# ab8898
Alexa Fluor 488 Goat anti-Rabbit cross-adsorbed	Thermo Fisher Scientific	cat# A11008
<i>Cy3 AffiniPure Donkey Anti-Rat IgG</i>	Jackson ImmunoResearch	cat# 712-165-150
Anti-digoxigenin-rhodamine, Fab fragments	Roche	cat# 11207750910
Mouse monoclonal anti-Piwi	Santa Cruz Biotechnology	cat#390946
Mouse monoclonal anti $\alpha$ -Tubulin	Abcam	cat#7291
<b>Chemicals, Peptides, and Recombinant Proteins</b>		
Trizol reagent	Thermo Fisher Scientific	cat# 15596026
Superscript III reverse transcriptase	Thermo Fisher Scientific	cat# 18080044
RNaseOUT Recombinant Ribonuclease Inhibitor	Thermo Fisher Scientific	cat# 10777019
dNTP mix (10mM each)	Thermo Fisher Scientific	cat# 18427013
Random hexamers (50 $\mu$ M)	Thermo Fisher Scientific	cat# N8080127
Pefabloc SC (AEBSF)	Roche	cat# 11585916001
cOmplete, EDTA-free Protease inhibitor Cocktail	Roche	cat# 05056489001
Gotaq G2 Hot Start Green Master Mix	Promega	cat# M7422
Gotaq G2 DNA Polymerase	Promega	cat# M7841
<b>Critical Commercial Assays</b>		
LightCycler 480 SYBR Green I Master	Roche LifeScience	cat# 04887352001
Turbo DNA free kit	Ambion	cat# AM1907
Dynabeads protein G	Thermo Fisher Scientific	cat# 10004D
HiTrap Q HP	GE Healthcare	cat# 17115301
Ribo-Zero rRNA Removal Kit (H/M/R)	illumina	cat#: MRZH116
RNA Clean & Concentrator-5	ZYMO RESEARCH	cat#: R1015
<b>Deposited Data</b>		
NGS_Raw and analyzed data	This paper	<a href="http://www.ncbi.nlm.nih.gov/geo/accession/number/GSE83238">http://www.ncbi.nlm.nih.gov/geo: accession number GSE83238.</a>
Original data	This paper	<a href="http://dx.doi.org/10.17632/gcckhsm8vg.1">http://dx.doi.org/10.17632/gcckhsm8vg.1</a>
<i>Drosophila melanogaster</i> reference genome NCBI	Genome Reference Consortium	Dm3
<b>Experimental Models: Organisms/Strains</b>		
<i>D. melanogaster</i> : RNAi of Piwi: y[1] sc[*] v[1]; P{TRiP.GL00626}attP40;	Bloomington Drosophila Stock Center	BDSC:37483; FlyBase: FBtp0070665
<i>D. melanogaster</i> : RNAi of Zuc: y[1] sc[*] v[1] ; ; P{TRiP. GL00112}attP2	Bloomington Drosophila Stock Center	BDSC:35228; FlyBase: FBtp006821
<i>D. melanogaster</i> : RNAi of White: y[1] v[1]; ; P{TRiP.HMS00017}attP2	Bloomington Drosophila Stock Center	BDSC:33623; FlyBase: FBtp0064645
<i>D. melanogaster</i> : conditional ubiquitous embryonic driver: y[*] w[*] vasa-GAL80 <sup>ts</sup> ; ;da-GAL4	This paper	Flybase: FBtp0001168
<b>Recombinant DNA</b>		
P{tubP-GAL80 <sup>ts</sup> }	Davis' laboratory	N/A
PattB	Bassler's laboratory	N/A

(Continued on next page)

<b>Continued</b>		
REAGENT or RESOURCE	SOURCE	IDENTIFIER
P3xp3-eGFP/vasa-phiC31.attB	Bischof et al., 2007	N/A
P3xp3-eGFP/nos-phiC31.attB	Bischof et al., 2007	N/A
PattB-vasa-GAL80 <sup>ts</sup>	This study	N/A
PattB-nanos-GAL80 <sup>ts</sup>	This study	N/A
Sequence-Based Reagents		
Primers for RT-qPCR, RT-PCR, CHIP-qPCR and riboprobe synthesis	SIGMA-ALDRICH or MWG	Table S2
Software and Algorithms		
Bowtie2	Langmead and Salzberg, 2012	<a href="http://bowtie-bio.sourceforge.net/bowtie2/index.shtml">http://bowtie-bio.sourceforge.net/bowtie2/index.shtml</a>
STAR (version bundled with piPipes)	Dobin et al., 2013	<a href="https://github.com/alexdobin/STAR">https://github.com/alexdobin/STAR</a>
Cufflinks (2.2.2)	Trapnell et al., 2010	<a href="http://cole-trapnell-lab.github.io/cufflinks">http://cole-trapnell-lab.github.io/cufflinks</a>
piPipes (commit cd5f1cfb33e67ddf2926cea7ad57212b17695e27)	Han et al., 2014	<a href="https://github.com/bowhan/piPipes.git">https://github.com/bowhan/piPipes.git</a>
Snakemake	Köster and Rahmann, 2012	<a href="https://bitbucket.org/johanneskoester/snakemake">https://bitbucket.org/johanneskoester/snakemake</a>
DeepTools (2.2.3)	Ramírez et al., 2016	<a href="https://github.com/fidelram/deepTools">https://github.com/fidelram/deepTools</a>
BWA (0.7.10-r789)	Li and Durbin, 2010	<a href="https://github.com/lh3/bwa">https://github.com/lh3/bwa</a>
TopHat(2.1.0)	Trapnell et al., 2009	
eXpress (1.5.1)	Roberts et al., 2011	<a href="http://bio.math.berkeley.edu/eXpress/index.html">http://bio.math.berkeley.edu/eXpress/index.html</a>
SciPy	Jones et al., 2001	<a href="http://www.scipy.org/">http://www.scipy.org/</a>

## CONTACT FOR REAGENT AND RESSOURCES SHARING

Further information and requests for reagents may be directed to, and will be fulfilled by the Lead Contact, Séverine Chambeyron ([severine.chambeyron@igh.cnrs.fr](mailto:severine.chambeyron@igh.cnrs.fr)).

## METHOD DETAILS

### *Drosophila* stocks

Fly stocks were maintained in standard conditions (25°C). The knock-down lines used in this study were from the Bloomington *Drosophila* Stock Center and are listed in the Key resources table.

### Construction of transgenic fly stocks

The thermo-sensitive GAL4 inhibitor (GAL80<sup>ts</sup>) with the 3' UTR of SV40 was PCR-amplified from the *P{tubP-GAL80<sup>ts</sup>}* plasmid (provided by Ronald L. Davis' laboratory). The resulting 1.4kb fragment was inserted in the *Not1* and *Xba1* restriction sites of the PattB vector to construct the PattB-GAL80<sup>ts</sup> vector. The 2.2kb fragment of the *vasa* and the 950pb fragment of the *nanos* promoters were obtained by *BamH1* and *Not1* digestion of the *P3xp3-eGFP/vasa-phiC31.attB* and *P3xp3-eGFP/nos-phiC31.attB* vectors, respectively (provided by K. Basler's laboratory) (Bischof et al., 2007). The *vasa* and the *nanos BamH1/Not1* fragments were inserted in the *BamH1* and *Not1* restriction sites of the PattB-GAL80<sup>ts</sup> vector. The resulting PattB-*vasa*-GAL80<sup>ts</sup> and PattB-*nanos*-GAL80<sup>ts</sup> plasmids were used by BestGene to generate the corresponding transgenic stocks with PhiC31-mediated transformation in the 2A3 landing site.

### Stage-specific depletion of the protein of interest during *Drosophila* development

#### Embryonic depletion

Females of the *vasa-GAL80<sup>ts</sup>;da-GAL4* recombinant stock were crossed with *UASp-shpiwi* or *UASp-shzuc* or *UAS-shwhite* males at 28°C. The progeny was collected for 13h at 28°C and kept for 3 more hours at 28°C, to knock down specifically the protein of interest in the germline for 3 to 16 hr, and then transferred to 18°C for the remainder of development (larvae, pupae) and adult life.

#### Larval depletion

Females of the *nanos-GAL80<sup>ts</sup>;nanos-GAL4-VP16* recombinant stock were crossed with *UASp-shpiwi* males at 18°C. The progeny was bred at 18°C throughout development except for a 48h shift at 28°C at the early larval stages (L1, L2).

#### Adult depletion

*vasa-GAL80<sup>ts</sup>;da-GAL4* females were crossed with *UASp-shpiwi*, *UASp-shrhi* or *UAS-shwhite* males at 18°C. Embryos, larvae and pupae were raised at 18°C. Newly emerged adults were shifted to 28°C for 5 days to inactivate the GAL80<sup>ts</sup> GAL4 inhibitor and induce adult Piwi, Rhi or White RNAi before ovarian dissection.

### Fertility test

After *shpiwi* or *shwhite* embryonic or larval expression, ten 3- to 5-day-old females were mated with five white<sup>1118</sup> control males at 20°C for 4 days. Four and five independent crosses were performed respectively. The number of adult offspring per cross was counted.

### RNA extraction and RT-qPCR

Total RNA was extracted with TRIzol following the manufacturer's instructions. RNA was DNase-treated. 1 μg of RNA was reverse transcribed using SuperScript III and random primers or the strand-specific primers listed in Table S2. Quantitative PCR analyses were performed with the LightCycler® 480 SYBR Green I Master system. RNA levels were calculated with the 2<sup>(-ΔΔCt)</sup> method (Livak and Schmittgen, 2001) using the *RpL32* housekeeping gene as reference. Data were analyzed with the LightCycler software. Each experiment was performed with biological triplicates and technical duplicates.

### Small RNA purification and sequencing

Small RNAs from ovaries were manually isolated on HiTrap Q HP anion exchange columns, as previously described (Grentzinger and Chambeyron, 2014). Library construction and 50nt single-read sequencing were performed using two biological replicates. One replicate (*piwi*-noKD, *white*-embKD and *piwi*-embKD libraries) was sequenced by Donnelly Sequencing Centre (Toronto) on an Illumina HiSeq2500 and the other (*white*-embKD-rep2 and *piwi*-embKD-rep2 libraries) by BGI (China) on an Illumina HiSeq 2500 instrument.

### ChIP-seq and ChIP-qPCR

ChIP was performed essentially as previously described (Mugat et al., 2015). Briefly, 100 dissected ovaries were crosslinked with 1.8% formaldehyde for 10 min, and the prepared chromatin was sonicated. One-third was used for immunoprecipitation with anti-H3K9me3 or -Rhi antibodies listed in the Key resources table. After de-crosslinking, DNA was extracted and used for qPCR measurements or library preparation for sequencing. Library preparation and 50nt single-read sequencing were performed by Donnelly Sequencing Centre (Toronto) on an Illumina HiSeq2500. The ChIP-seq experiments were performed on two biological replicates for the *piwi*-embKD and on three biological replicates for the *white*-embKD. The analyses presented here were performed using pooled biological replicates. Primers for ChIP-qPCR are listed in Table S2.

### RNA-seq

Strand-specific RNA-seq was performed as previously described (Zhang et al., 2012). Briefly, total RNA was extracted from ovaries using TRIzol. 4 μg of total RNA was subjected to Ribo-Zero ribosomal depletion. RNA was further purified using RNA Clean & Concentrator-5. Library construction and 150nt paired-end read sequencing were performed by Donnelly Sequencing Centre (Toronto) on an Illumina NextSeq 500 apparatus. The RNA-seq experiments were done using two biological replicates.

### RNA fluorescent in situ hybridization and immunofluorescence

RNA FISH and immunofluorescence experiments were carried out according to previously described procedures (Grentzinger et al., 2012). In brief, female gonads or ovaries were dissected in PBS from third instar larvae or 3-5 day old females and fixed in fixation buffer (4% formaldehyde 0.3% Tween 20 and 1x PBS) for 20 min. After permeabilization with 1% Triton X-100/1x PBS for 30 min, ovaries were blocked with blocking buffer (1% BSA, 0.3% Tween20, 1x PBS) for 30 min before incubation with primary antibodies.

For embryo staining, flies were caged and fed yeast paste. Embryos (3-16h) were collected, dechorionated in 50% bleach, and fixed in PBS, 50mM EGTA, 8% formaldehyde and heptane for 25 min, devitellinized by vigorous shaking in methanol, and washed in PBS with 0.1% Tween-20. The primary antibody dilutions for immunostaining were 1:500 for anti-Piwi and 1:400 for anti-Vasa antibodies. The secondary antibodies were goat anti-rabbit Alexa488 (1:400) and donkey anti-rat Cy3 (1:200).

### Western blot analysis

50 μg of proteins extracted from late embryos (16 AEL) from each sample were loaded on precast gels (Bio Rad). Anti-α-Tubulin (1:5000 dilution) and Anti-Piwi (1:1000).

### Computational Analysis

#### Small RNA-seq

Raw reads were trimmed from their 3' linkers. Trimmed reads (18-30nts in size) were mapped with Bowtie2 using mismatch-tolerant settings to the *Drosophila melanogaster* genome (Release 5; dm3) complemented with canonical transposable elements (TEs). Reads were annotated based on their mapping coordinates. Candidate piRNAs were 23 to 30nt reads that mapped to regions annotated as piRNA clusters (Brennecke et al., 2007), TEs (*Drosophila* consensus TE sequences taken from <https://github.com/cbergman/transposons>) or 3'UTRs (<ftp://ftp.flybase.net/>), but not to other regions. Unique mappers were defined as reads for which only one best-score alignment existed in the genome. Candidate piRNAs were mapped again to piRNA cluster sequences and canonical TE sequences. Data were normalized using the number of miRNA reads determined during the primary annotation (<ftp://ftp.flybase.net/>) or using the unique mapper reads of the flamenco cluster. For pileup representations, reads the 5' end of which mapped to a given position were counted. Our full analysis pipeline is available at <https://bitbucket.org/blaiseli/pirna-pipeline>.

### ChIP-seq

To determine the H3K9me3 profile at transposable element sequences, we used the ChIP-seq pipeline of the piPipes package (<https://github.com/bowhan/piPipes.git>, commit cd5f1cfb33e67ddf2926cea7ad57212b17695e27) (Han et al., 2014) with the recommended settings [-B (broad peak) -m (use both unique and multi-mappers; for multi-mappers, Bowtie2 randomly reports one locus from the best alignment pool)] and the *Drosophila melanogaster* genome (Release 5; dm3). Coverage was normalized by sequencing depth (RPM). We modified the piPipes pipeline to plot the H3K9me3 enrichment relative to input along each of the 126 studied transposable elements using a pseudo-count of 1 at each nucleotide position.

For piRNA cluster analysis, 50bp single-end reads were mapped to the *Drosophila melanogaster* genome (Release 5; dm3) with BWA. DeepTools 2.0 was used to generate bigwig files of H3K9me3 IP and Input (bamCoverage), IP/Input ratio (bigwigCompare) and meta-piRNA cluster matrices (computeMatrix). We have extended reads to fit the average fragment length (-extendReads 200), filter PCR duplicates (-ignoreDuplicates), keep high-quality mapped reads (and uniquely mapped) (-minMappingQuality 20) and normalize coverage by sequencing depth (-normalizeUsingRPKM). The bigWig files used for the downstream analysis were generated at 10bp resolution bins (-binSize 10). The piRNA cluster coordinates were taken in bed format from (Brennecke et al., 2007) to make meta-piRNA cluster matrices of H3K9me3 enrichment (computeMatrix scale-region). Because of differences in length of such regions, we decided to cut the body of every region by 2000 bins and used the mean of signal. Three biological replicates for the white-embKD and two for the piwi-embKD condition were merged to increase the signal and statistical power. Indeed, the replicates were similar, as verified with the Spearman's correlation testing of piRNA cluster regions (data not shown). A homemade R script was then used to generate boxplots and for pairwise Wilcoxon test analysis with the matrix described above. This pipeline used a dedicated workflow system called snakemake (Köster and Rahmann, 2012) and is available upon request.

### RNA-seq

Genome-wide quantification of the steady state RNA levels was done by RNA-seq using piPipes from github (<https://github.com/bowhan/piPipes.git>, commit cd5f1cfb33e67ddf2926cea7ad57212b17695e27), the RNA-seq pipeline for transcriptome analyses. Briefly paired-end reads were aligned to rRNA with Bowtie2 (Langmead and Salzberg, 2012). STAR (Dobin et al., 2013) was used to align the resulting unmapped reads to the *Drosophila melanogaster* genome (Release 5; dm3). The mapping results were then processed with Cufflinks (Trapnell et al., 2010) to determine the normalization factor based on reads that mapped to genes. Reads were then mapped to gene and transposon sequences using Bowtie2 and the mapping results were processed with eXpress (Roberts and Pachter, 2011) for quantification. Quantification by eXpress was then normalized using the Cufflinks-determined normalization factor.

BigWig files for IGV genome browser contain only unique mappers and were normalized to the library depth, which is calculated by Cufflinks (RPM). For boxplots, the homemade R script was used and the RNA-seq reads mapped to dual-strand piRNA clusters (extracted from Brennecke et al., 2007) and normalized by depth and cluster size (RPKM). Paired Wilcoxon test was used for comparisons.

Pairwise comparison of piRNA cluster splicing: for each gene or piRNA cluster, TopHat (TopHat v2.1.0) (Trapnell et al., 2009) was used to compute the number of reads that mapped to potential exon-exon junctions. This number was normalized to the length of the gene or piRNA cluster and a pseudo-count of 0.001 read per kilobase was added. The spliced reads ratio (SRR) between two RNA-seq libraries was calculated for each gene or piRNA cluster and the distributions of the cluster and gene SRRs were compared using the Wilcoxon rank-sum test (implemented in the SciPy library) (<https://www.scipy.org/citing.html#scipy-the-library>). The medians of the gene and piRNA cluster SRR distributions were calculated and the median piRNA cluster SRR was normalized to the median gene SRR.

## QUANTIFICATION AND STATISTICAL ANALYSIS

Unless otherwise specified, statistical analyses for ChIP-qPCR, RT-qPCR were performed using the SciPy library (<https://www.scipy.org/citing.html#scipy-the-library>). P values were calculated using two-tailed Student's t tests for samples displaying normal distribution (tested with the Shapiro-Wilk test). Variance homogeneity was tested with the Levene's test. When at least one of the two series did not have a normal distribution, P values were calculated using the Mann-Whitney rank-sum test (with correction for continuity).

The pairwise Wilcoxon test was used for both ChIP-seq and RNA-seq analyses and the Wilcoxon rank-sum test (implemented in the SciPy library) for the pairwise comparisons of piRNA cluster splicing.

## DATA AND SOFTWARE AVAILABILITY

The accession number for the sequencing data reported in this paper is NCBI Gene Expression Omnibus (GEO) (<http://www.ncbi.nlm.nih.gov/geo/>): GSE83238. Original data are available via Mendeley: <http://dx.doi.org/10.17632/gcckhsm8vg.1>. The accession number for the ChIP-seq data from Piwi-GLKD and control ovaries reported in this paper is GEO: GSE55824. The accession number for the RNA-seq data from *Rhi*-mutant, Oregon-R and w<sup>1</sup> reported in this paper is GEO: SRP030460.

**Molecular Cell, Volume 66**

**Supplemental Information**

**Piwi Is Required during *Drosophila* Embryogenesis  
to License Dual-Strand piRNA Clusters for  
Transposon Repression in Adult Ovaries**

**Abdou Akkouche, Bruno Mugat, Bridlin Barckmann, Carolina Varela-Chavez, Blaise Li, Raoul Raffel, Alain Pélisson, and Séverine Chambeyron**

Figure S1

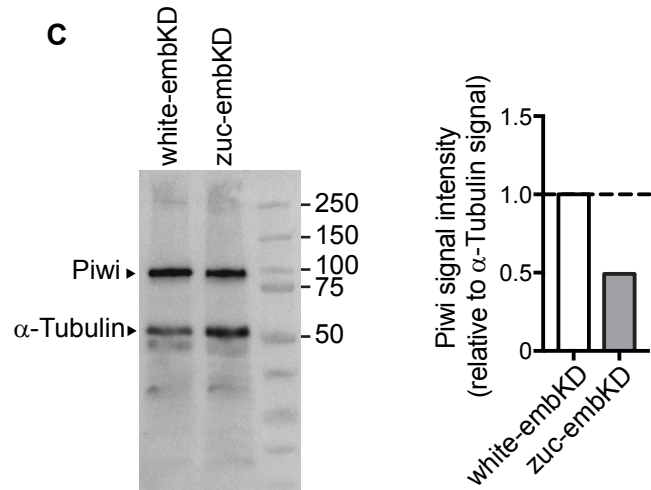
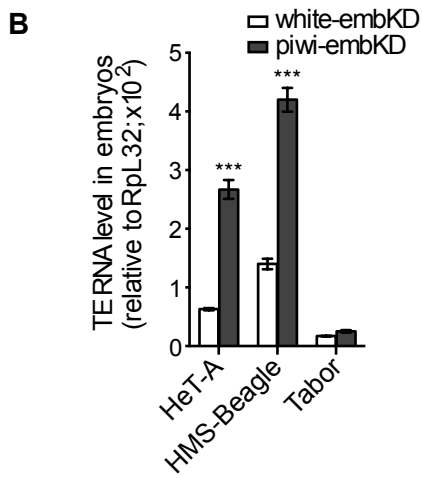
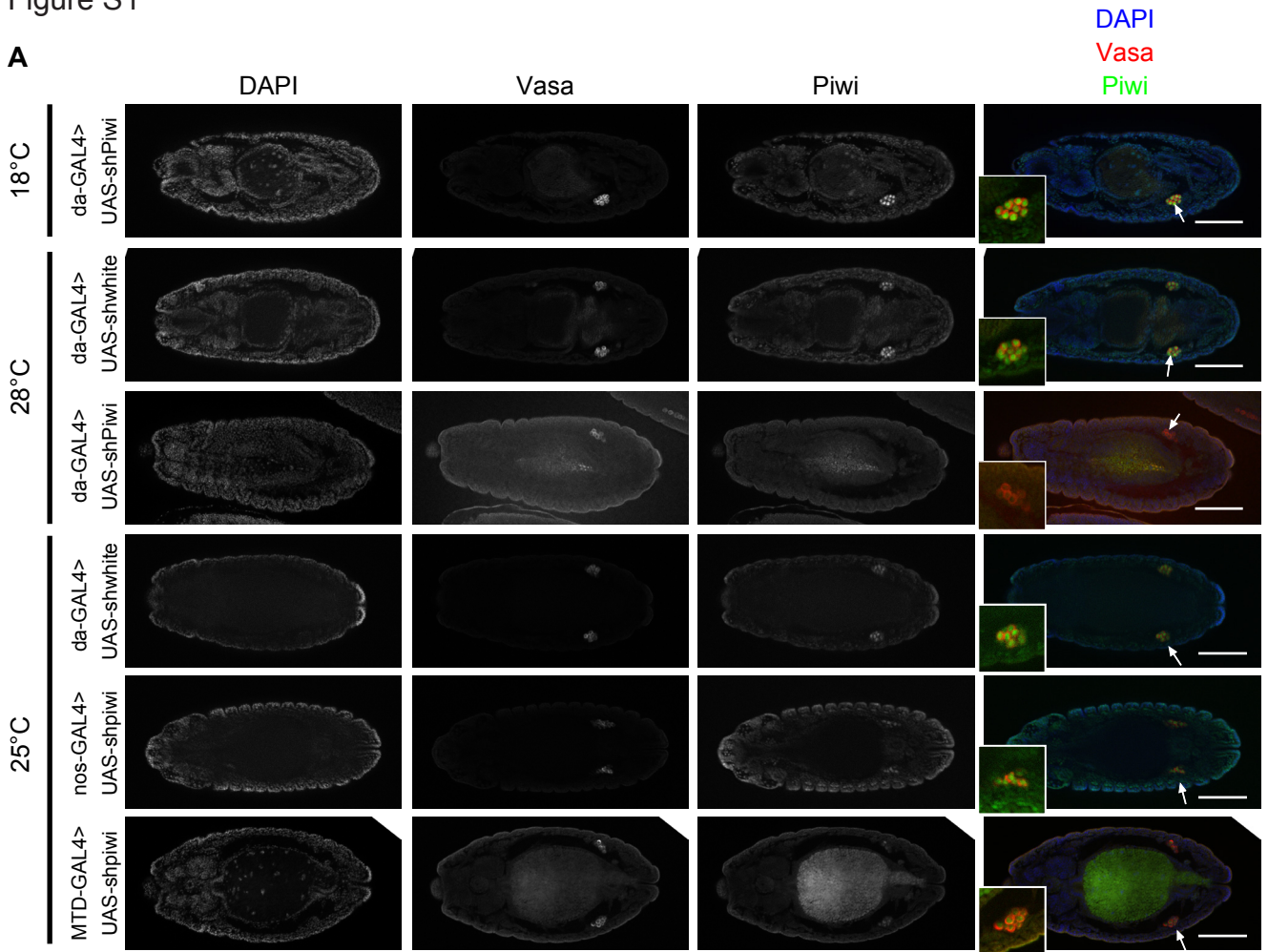


Figure S1: Related to Figure 1

(A) Immunofluorescence analysis of Piwi (green) and Vasa (red) expression in germinal cells of stage 13-14 *Drosophila* embryos. Upper panels: *da-GAL4>UAS-shpiwi* (piwi-noKD) at 18°C; middle panels: *da-GAL4>UAS-shwhite* (white-embKD) and *da-GAL4>UAS-shpiwi* (piwi-embKD) at 28°C; lower panels: *da-GAL4>UAS-shwhite*, *nos-GAL4>UAS-shpiwi* and *MTD-GAL4> UAS-shpiwi* at 25°C. DNA was labeled with DAPI (blue). Insets: Detailed view of one embryonic gonad. Arrows indicate the embryonic gonad. Scale bar, 100 μm.

(B) Steady-state RNA levels of germline-dominant (HeT-A and HMS-Beagle) and soma-dominant (Tabor) TEs in total RNA from white-embKD and piwi-embKD embryos (12h after egg laying (AEL)), determined by RT-qPCR. Data are the mean ± SD of three biological replicates; \*\*\*: *P*-value <0.005 (two-tailed Student's *t* test). (C) Western blot showing protein levels of Piwi and α-Tubulin in white-embKD and Zuc-embKD embryos (16h to 20h AEL). A quantification of the Piwi signal relative to the α-Tubulin signal is shown on the left panel. This quantification was done using ImageJ software.

Figure S2

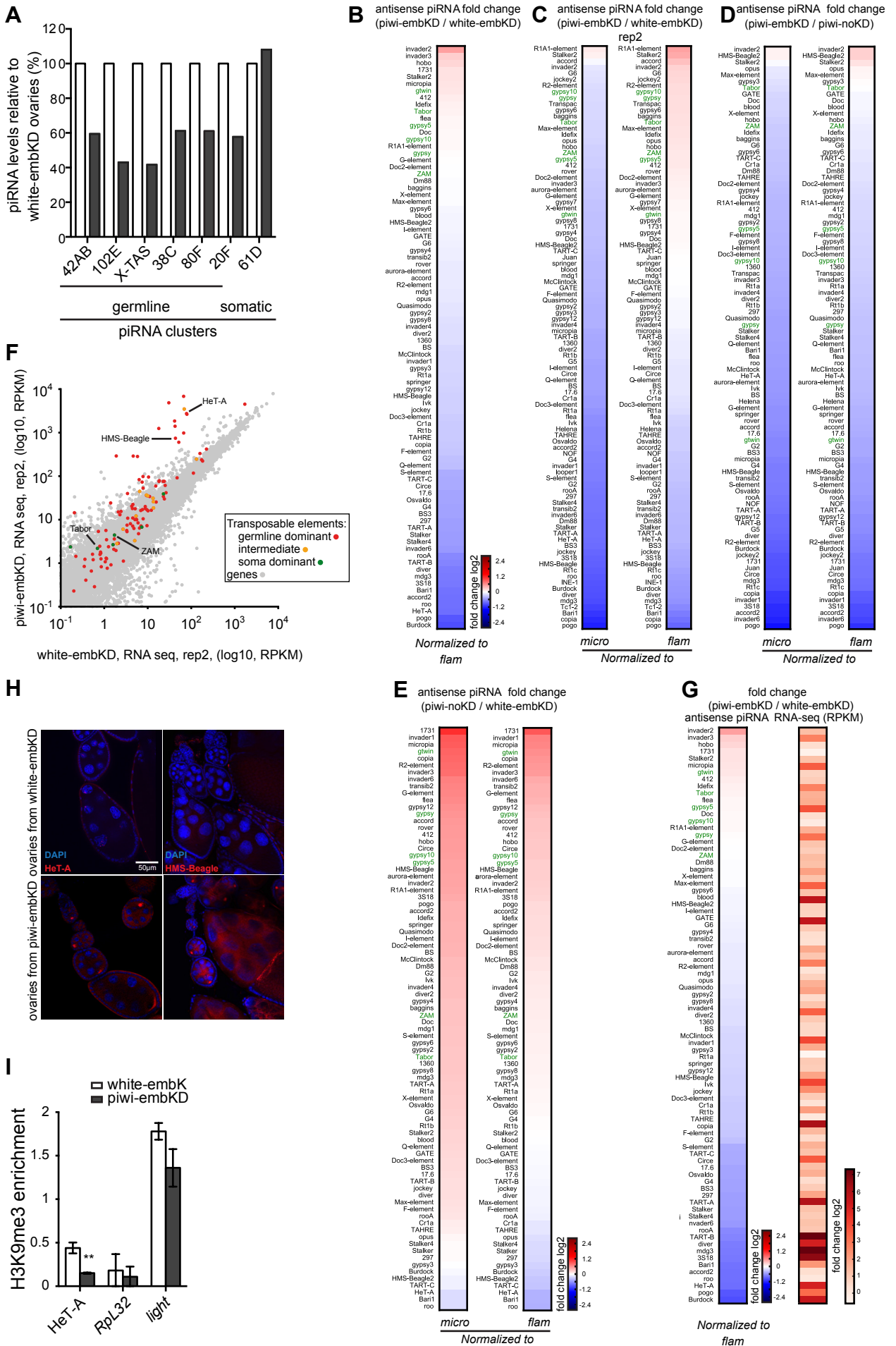


Figure S2: Related to Figure 2

(A) Same legend as in Figure 2A except that the piRNA levels were normalized to flamenco unique mapper reads. (B) Heat map representing the fold change of antisense TE piRNA accumulation in piwi-embKD *versus* white-embKD ovaries, like for Figure 2B except that it was normalized to flamenco unique mapper reads. (C-E) Same legend as in Figure 2B except that the analysis was performed using two other white-embKD and piwi-embKD biological replicates (rep2) (C), piwi-embKD and piwi-noKD ovaries (D) and piwi-noKD and white-embKD (E) normalized to miRNA reads (left panel) or to flamenco unique mapper reads (right panel). (F) Same legend as for Figure 2C except that in this experiment we compared two other white-embKD and piwi-embKD biological replicates (rep2). (G) Heat map representing a pairwise comparison of the fold change of antisense TE piRNAs (left: duplication of Figure S2B) with the fold change of TE RNA-seq normalized signal (right) in piwi-embKD *versus* white-embKD ovaries. (H) RNA FISH of whole-mount ovaries after white (upper panels) or piwi (lower panels) embryonic knock-down using a rhodamine-conjugated antibody against digoxigenin antisense riboprobes that target HeT-A and HMS-Beagle. Sense transcripts for these two germline-dominant TEs were detected (red) only after piwi embryonic knock-down. DNA was labeled with DAPI (blue). (I) ChIP-qPCR quantification of H3K9me3 enrichment at the HeT-A transposable element in ovaries. The *RpL32* and *light* genes were used as examples of actively transcribed genes localized in euchromatic and in heterochromatic regions, respectively. H3K9me3 enrichment was quantified relative to the 1360-element (positive control) and normalized to input (mean  $\pm$  SD of three biological replicates); \*\**P*-value <0.05 (two-tailed Student's *t*-test).

Figure S3

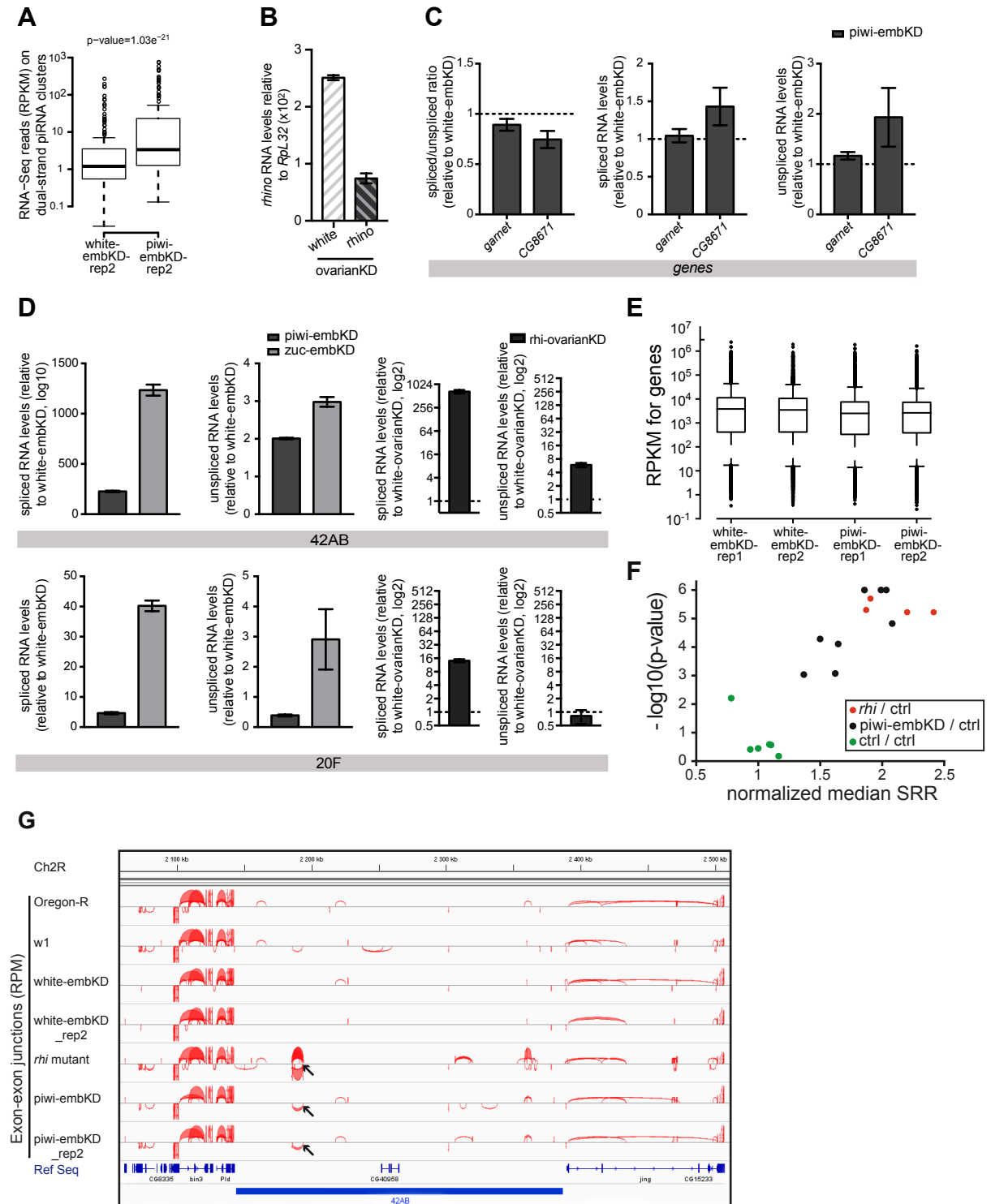


Figure S3: Related to Figure 3

(A) Box-plots showing the distribution of normalized RNA-seq signals (Reads Per Kilobase per Million mapped reads, RPKM) at bins belonging to dual-strand piRNA clusters in white-embKD-rep2 and piwi-embKD-rep2 ovarian samples;  $P$ -value =  $1.03e^{-21}$  (pair-wise Wilcoxon test). (B) Steady-state levels of *rhi* RNA in white-ovarianKD and *rhi*-ovarianKD ovaries determined by RT-qPCR and normalized to the expression of the *RpL32* house-keeping gene. (C) Splicing assayed by RT-qPCR at two spliced sites located in the *garnet* and *CG8671* genes. The unspliced and spliced amplicons were quantified relative to *RpL32* in piwi- or white-embKD ovaries and the spliced/unspliced ratios were normalized to the ratio of the white-embKD control experiment (mean  $\pm$  SD of three biological replicates). (D) RT-qPCR assays to assess splicing of transcripts isolated from piwi-embKD, zuc-embKD and white-embKD ovaries and from *rhi*-ovarianKD and white-ovarianKD ovaries at the 42AB cluster (upper panels) and the 20F cluster (lower panels). The spliced and unspliced amplicons were quantified relative to *RpL32* expression and then normalized to the white-embKD or to white-ovarianKD control. Data are the mean  $\pm$  SD of three biological replicates. (E) Boxplot showing the number of RNA-seq reads that mapped to putative exon-exon junctions of coding genes in white-embKD and piwi-embKD ovaries (two biological replicates are shown). The number of reads was normalized by the library depth and the gene length. (F) Pair-wise strain comparisons of the spliced read ratios (SRRs) of transcripts from dual-strand piRNA clusters normalized to the SRRs of transcripts from coding genes. On the y axis are represented, in a log<sub>10</sub> scale, the  $P$ -values (Wilcoxon test comparisons) of the comparison between "cluster" and "gene" SRR distributions for each pair of strains (for graphical clarity,  $p$ -values  $<10^{-6}$  were collapsed to  $10^{-6}$ ). On the x axis is indicated the median of the "cluster" SRR distribution normalized to the median of the "gene" SRR distribution. Green dots: the six pair-wise comparisons of the four wild-type control ovarian RNA-seq libraries [Ore-R and w1 (ovarian RNA-seq libraries previously described in Zhang et al., 2014), white-embKD and white-embKD-rep2). The normalized median SRRs were close to 1, indicating that the number of piRNA cluster spliced reads did not significantly differ among the four libraries. Red dots: comparison of each of these four control libraries with the previously published library obtained from *rhi* mutant ovaries (Zhang et al., 2014). The normalized median SRRs were between 1.8 and 2.4 ( $P$ -values  $<10^{-5}$ ), confirming that Rhi depletion has a significant positive effect on piRNA cluster splicing. Black dots: all pair-wise comparisons of the four wild type libraries with the two piwi-embKD ovarian RNA-seq libraries (piwi-embKD and piwi-embKD-rep2). These comparisons indicated that Piwi depletion from embryos had a significant ( $P$ -values  $<10^{-3}$ ) positive effect on piRNA cluster splicing (normalized median SSRs between 1.3 and 2.1). (G) IGV Genome Browser screenshot of cluster 42AB displaying RNA-seq reads of exon-exon junctions defined by TopHat and normalized by depth (reads per million: RPM) and mapped to the Watson (+: up) and Crick (-: down) orientation. Arrows indicate the splicing site studied in Figure 3C.

Figure S4

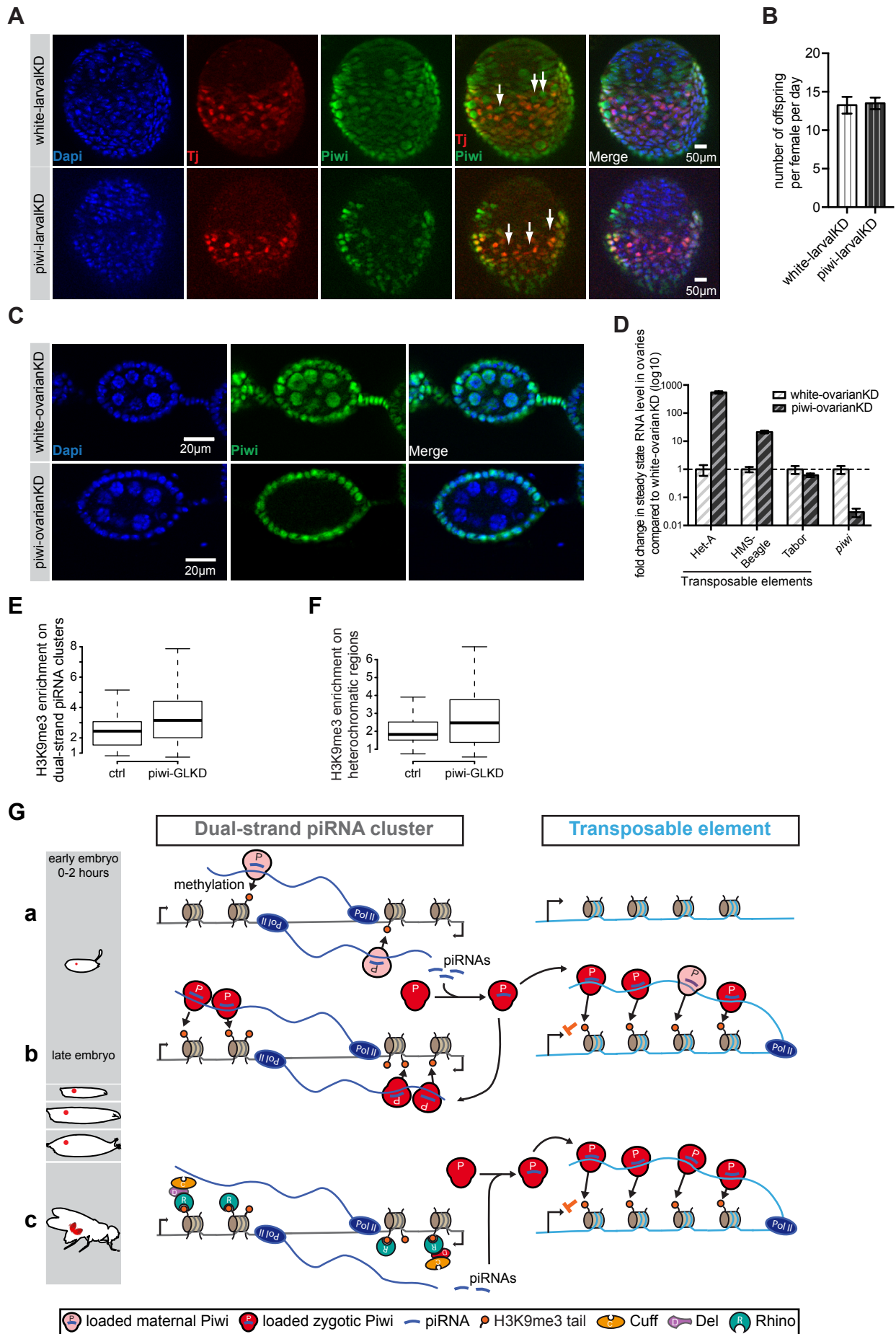


Figure S4: Related to Figure 4

(A) Immunostaining of Piwi (green) and Traffic jam (Tj) (red) in third instar larval gonads after white or piwi transient germinal RNAi. DNA was labeled with DAPI (blue). Some examples of germline nuclei are indicated by arrows. (B) Number of offspring produced per female per day after transient knock-down of *piwi* (piwi-larvalKD) or *white* (white-larvalKD) in larvae. Histograms represent the mean  $\pm$  SD of five biological replicates. (C) Immunostaining of Piwi (green) in ovaries after white or piwi transient germinal RNAi. DNA was labeled with DAPI (blue). (D) Fold-change of TE and *piwi* steady-state RNA levels analyzed by RT-qPCR upon *white* or *piwi* ovarian knock-down. Quantification was done relative to *RpL32* and normalized to the white-ovarianKD experiment. (E-F) Box-plots showing the distribution of ovarian H3K9me3 enrichment at dual-strand piRNA cluster sequences (E), and non-piRNA-cluster heterochromatic regions (F) after control or Piwi germinal depletion (piwi-GLKD) using previously published ChIP-seq data (Mohn et al., 2014). See Figures 1D-E for details. (G) A working model of Piwi-dependent dual-strand piRNA cluster licensing in the embryo. (a) Putatively unstable licensing of piRNA clusters by maternal Piwi deposited in early embryos. It is assumed that maternal Piwi-associated piRNAs modify the chromatin of dual-strand clusters *via* base pairing with nascent transcripts produced before the onset of general zygotic transcription. (b) Stable piRNA cluster licensing by Piwi expressed in the embryo (zygotic Piwi). The early partial licensing of piRNA clusters by maternal Piwi would allow the production of enough zygotic piRNAs to be loaded by the zygotic Piwi proteins that could thus deposit additional H3K9me3 marks, leading to fully functional dual-strand piRNA clusters. These zygotic Piwi-loaded piRNAs are also involved in TE silencing during embryogenesis. (c) Piwi-independent maintenance of piRNA cluster licensing throughout development and adult life. The co-transcriptional recruitment of the RDC complex, *via* Rhi binding to the H3K9me3 marks inherited in a Piwi-independent manner, would lead to the unconventional transcription of dual-strand piRNA clusters (splicing inhibition, read-through transcription...) that is required for productive piRNA precursor biogenesis during oogenesis.

SUPPLEMENTAL TABLES

Table S1: Small RNA library annotation: Related to Figure 2

	piwi-noKD	piwi-embKD	white-embKD	white-embKD_rep2	piwi-embKD_rep2
Category	Number of reads	Number of reads	Number of reads	Number of reads	Number of reads
small_RNA_reads	33167167	50228799	35980570	35612711	36578878
mappers	33015499	49315628	35751227	34538941	36042769
rRNA	25546150	5054786	27188336	1044884	758968
tRNA	36474	136540	100969	62733	63825
snoRNA	27017	291388	85941	60012	49566
ncRNA	21011	30661	121807	15037	16422
5'UTR	32353	97797	87764	136479	79049
CDS	355414	888250	1109373	1021818	738184
miRNA	1997369	17469879	2346465	8905286	13281280
siRNA	123186	677926	124423	489603	818754
piRNA	4076985	20134472	3413090	19145652	16097387

Table S2: Primers : Related to Figure 1;2;3 and 4

Primers for RT-qPCR to measure the splicing ratio: Related to Figure 3

Name	Sequence
42AB-RT	(Zhang et al., 2014)
42AB-Left	(Zhang et al., 2014)
42AB-Right-Spliced	(Zhang et al., 2014)
42AB-Right-Unspliced	(Zhang et al., 2014)
Rpl32-RT	GGAGGAGACGCCG
Rpl32-Left	(Zhang et al., 2014)
Rpl32-Right	(Zhang et al., 2014)
20F-RT	TTATGCCCACTTTTGTGTGTC
20F-Left	CCAGGGACGTCTCATCCTAC
20F-f	TGCGTGACACCCAAGAAA
20F-Right-Spliced	CGTCGCTAGTCTAAGCGC
20F-Right-Unspliced	GTTTCAAGAAGTCACCTCGC
cg8671-intron1 spliced-f	CAAACGAAAGCAAAGGCAGTTG
cg8671-intron1 spliced-r	ATATAGCGGAGACACATCCGAA
cg8671-intron1 unspliced-f	TGTTCCGTGCTGTTGTGTTTGT
cg8671-intron1 unspliced-r	ATATAGCGGAGACACATCCGAA
garnet-intron7 spliced-f	CCTTAGAACCCCGGCTAGGAAA
garnet-intron7 spliced-r	CAGAGCTGAATGGAGGCACTGT
garnet-intron7 unspliced-f	CGAACCAAAAACCAAAACCAAC
garnet-intron7 unspliced-r	CAGAGCTGAATGGAGGCACTGT

Primers for ChIP-qPCR: Related to Figure 1 and Figure 4

Name	Sequence
42AB-1-f/c11-A-f	CGTCCCAGCCTACCTAGTCA (Klattenhoff et al., 2009)
42AB-1-r/c11-A-r	ACTTCCCGGTGAAGACTCCT (Klattenhoff et al., 2009)
42AB-2-f/c11-B-f	GCAGATGAGCTGAAACGAAA (Klattenhoff et al., 2009)
42AB-2-r/c11-B-r	TCGCAGTCGTGTAATCCAAA (Klattenhoff et al., 2009)
80F-f	CACCTCCTGCGGTAATTCTCGC
80F-r	GAGTTCGAAGAGCTGGACACCC
Het-A	(Klenov et al., 2011)
18S-f	TTCATGCTTGGGATTGTGAA

<i>18S-r</i>	GTACAAAGGGCAGGGACGTA
<i>Light</i>	(Klenov et al., 2011)

Primers for qPCR: Related to Figure 1 and Figure2

Name	Sequence
piwi-f	GCGCTTTTAACCACCGTTTA
piwi-r	GGTCTCTGAAGTGCCTTTGC
rpl32-f	CCGCTTCAAGGGACAGTATCTG
rpl32-r	ATCTCGCCGCAGTAAACGC
HeT-A-f	CGCGCGGAACCCATCTTCAGA
HeT-A-r	CGCCGCAGTCGTTTGGTGAGT
HMS-Beagle-f	AATGCCCTTGTCGGACACGA
HMS-Beagle-r	TGATGAAACACATTACCAGAACCTTGA
Zam-f	CTACGAAATGGCAAGATTAATTCCACTTCC
Zam-r	CCCGTTTCCTTTATGTCGCAGTAGCT
Tabor-f	ACGTTGTTACGACATTAGCCG
Tabor-r	GGGTTGGTTCGGATCTGACG

Primers for riboprobe synthesis : Related to Figure 2

Name	Sequence
HeT-A probe-f	CAGGTCGGCAATGACAG
HeT-A probe-r	GGTAATACGACTCACTATAGGCAGTGCGTTCAGGATTGG
HMS-Beagle probe-f	TGATGAAACACATTACCAGAACCTTGA
HMS-Beagle probe-r	TAATACGACTCACTATAGGGAATGCCCTTGTCGGACACGA